Energy & Environmental Science

Accepted Manuscript

ROYAL SOCIETY OF CHEMISTRY

www.rsc.org/ees

Metal-Organic Frameworks and their derived nanostructures for Electrochemical Energy Storage and Conversion

Wei Xia,[a,1] Asif Mahmood,[a,1] Ruqiang Zou,[a,*] and Qiang Xu[b,*]

[a] Department of Materials Science and Engineering, College of Engineering, Peking University, Beijing 100871, China. E-mail: rzou@pku.edu.cn

[b] National Institute of Advanced Industrial Science and Technology (AIST), Ikeda, Osaka 563-8577, Japan. E-mail: q.xu@aist.go.jp

[1] W. X. and A. M. contributed equally to this work.

Outline

1. Introduction
2. Designing MOFs
3. Derivation of various structures from MOFs
    - 3.1. Carbons
    - 3.2. Metal Oxides
    - 3.3. Metal Oxide/Carbon Composite
    - 3.4. Metal-Nanoparticle@MOFs
4. Electrochemical Energy Storage Applications
    - 4.1. Supercapacitors
    - 4.2. Batteries
        - 4.2.1. Anode Materials
        - 4.2.2. Cathode Materials
    - 4.3. Fuel Cells
        - 4.3.1. Oxygen Reduction Reaction Catalysts
        - 4.3.2. Hydrogen/Oxygen Evolution Reaction Catalysts
        - 4.3.3. Electrolytes
5. Summary and Prospective

Abstract

Metal-organic frameworks (MOFs) have drawn tremendous attentions due to diverse structures, tunable properties and multi-applications like gas storage, catalysis and magnetism. Recently, there is a rapidly growing interest in developing MOF-based materials for electrochemical energy storage. From the recent progress, MOFs have proved to be particularly suitable for electrochemical application because of the tunable chemical composition that could be designed at molecular level and highly porous framework in which fast mass transportations of the related species are favorable. In this review, we present the recent progress in fabricating MOFs and MOF-derived nanostructures for electrochemical applications. We will sequentially introduce the principle and strategy of designing targeted MOFs followed by a highlight of some MOF-derived novel structures and their potential applications in electrochemical energy storage and conversion. Furthermore, major challenges in the electrochemical energy storage are discussed with prospective solutions in the light of current progress in MOF-based nanostructures.

1. Introduction

The storage of energy to light up portable electronic devices needs improvements in design and execution of materials, which has become a huge concern in recent research communities. Advent of nanotechnology with modern characterization facilities has triggered the conquest towards rational design of these materials. Electrochemical energy storage has been considered as one of the most promising

methods of storing energy. The optimization of nanostructured electrode for electrochemical energy storage needs systematic approach to harvest the maximum efficiencies.[1] Active surface area, optimized pore size distribution and crystallinity are considered to be the most important factors affecting the performance of nanoporous electrode materials.[2] Many materials have been investigated in search of the best materials for electrochemical energy storage lately including metal-organic frameworks (MOFs), however, an efficient design still remains a big challenge.

MOFs are highly porous materials which were first defined in late 1990s by Yaghi and coworkers.[3] These materials are extremely light (~0.13 g/cm^3) with very high surface areas (up to 10,000 m^2/g), large pore volumes and well-defined pore size distributions.[4] The surface areas of MOFs are much more than those of other porous materials such as zeolites and carbons. MOFs are formed by linking organic and inorganic moieties through coordination covalent linkages. Other types of interactions such as H-bonding, π-π stacking and Van der Waals forces may also play role in forming three-dimensional (3D) structures of MOFs. Till now, more than 20,000 MOFs have been discovered and studied for various applications in last decade.[4] MOFs could have pore size as large as 9.8 nm[5,6] under efficient control over interpenetration of MOF chains,[7] which improves their potential applications substantially. The pore sizes can be enlarged by increasing the length of organic ligand; however it usually accompanies interpenetration of the MOF chains. Researchers introduced the liquid phase epitaxy method to solve this critical issue.[7] This controlled synthesis route provides excellent opportunity to produce MOFs for

drug delivery and imaging,[8,9] optoelectronics,[10,11] proton conduction,[12,13] gas storage/separation[14-16] and catalysis.[17-19] Several MOFs have also been explored for their application in various electrochemical applications such as supercapacitors,[20] batteries[21] and fuel cells.[22] Although pristine MOFs were demonstrated "not suitable for application in reversible lithium storage",[23] subsequent works addressed this issue and demonstrated MOFs as efficient energy storage materials.[24-27] Apart from direct utilizations, MOFs have been used as supports to either load active nanomaterials for energy conversion reactions[28] or sacrificial materials to derive various nanostructures by different treatment methods (**Scheme 1**).[29] For example, we recently demonstrated an efficient method to produce nitrogen doped high surface area carbon from MOF and investigated their excellent carbon dioxide (CO_2) uptake and performance for oxygen reduction reaction (ORR).[30] Similarly, nanostructured electrodes call for high surface area with the maximum exposure of active sites to the electrolyte in order to obtain better performance. Since MOFs consist of metals and organic species, heating in air leads to MOF decomposition and formation of metal oxides (MO) with high surface areas that are suitable for electrochemical applications including batteries and supercapacitors.[31] Moreover, similar heating route can be effectively used to derive metal/metal oxide (M/MO) decorated high surface area carbonaceous materials for high performance electrochemical applications. Given the recent progress in MOF field, a number of nice reviews addressing advancements from synthesis[32-38] to various applications including catalysis,[39,40] throughput studies,[41] luminescence,[42] gas storage,[43] proton conduction,[44,45] electronic and optoelectronic devices,[46] adsorptive

separations,[47] and clean energy[48] have been published. Despite considerable advancement in the electrochemical application of MOFs,[45,49,50] the field is lacking a comprehensive review on electrochemical applications which can put together all the scattered data and provide a basis for future research in this very important field. This has led to poor understanding of different inter-related applications of these novel materials. For example, MOFs were considered poor conductors, however several recent reports suggest excellent proton conduction in MOFs. MOFs are efficiently packed crystalline materials but conduction is facilitated by less packed materials. So a borderline needs to be defined for meaningful future research on this subject. Similarly, several types of carbon materials have been derived from MOFs by decomposition at elevated temperatures for applications in batteries, supercapacitors and fuels cells, but a clear understanding of the carbonization process of these porous materials, especially the nature of resulting structures still remains unclear. MOs have been reported to have high theoretical and experimental capacities in batteries and supercapacitors, however they lack major progress due to the rigid structures. Recently, MOFs have been used to derive high surface area MOs, which does provide some space for solid electrolyte interphase (SEI) film formation providing better capacity retention. Recently, the derivation of MO doped carbonaceous material (MO@C) from MOFs has also addressed these issues in electrochemical applications. Using MOFs, highly porous MOs and MO@C could be prepared, which fulfill the requirements of homogenous dispersion of metallic species in the carbonaceous matrix and also provide a carbon coating on these metal oxide nanoparticles which

prevent their agglomeration, thus providing ideal sacrificial materials for synthesis of nanostructured electrode materials for electrochemical applications. In this review, we put the recently published data on electrochemical application of MOFs and MOF derived materials together pointing out the major hurdles in the development of this particular field and their prospective solutions.

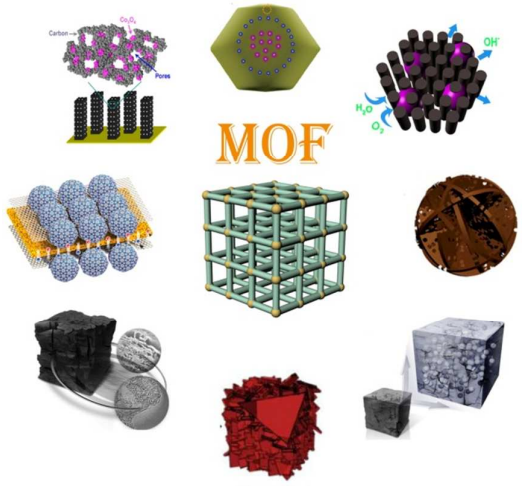

Scheme 1. MOFs based nanostructures.

2. Designing MOFs

Since MOFs can be designed according to desired structures, it is really important to understand the needs of particular applications to tailor the application oriented synthesis as has been demonstrated in several applications.[51-57] Electrochemical energy storage in pristine MOFs depend mainly on the design of the nanostructure (particle size, active surface area, pore size distribution, crystallinity and availability of functional groups for efficient conductivity) and their response towards changes in the local environment (e.g. reversible insertion of Li^+ ions in case of lithium ion batteries,

LIBs).[58,59] A major design issue is to address the level of porosity in the framework. Highly porous compounds based on MOFs could lead to cross over of fuel in the cells and deteriorate the performance.[44] MOFs exhibit both rigid and flexible structures which could be tuned to optimize the conductivity of MOF structures as well. Tremendous amount of research has been carried out to tailor the abundant carbon nanostructures for energy storage. Pioneering work has been done to identify the critical parameters (pore size and surface area) needed to tailor electrode materials for capacitive energy storage as shown in **Figure 1a**.[60,61] Similarly, the effect of pore size and wall thicknesses (distortion upon intercalation of Li^+ as shown in **Figure 1b**) on reversible insertion of Li^+ for high performance LIBs was further elaborated.[62] Keeping in view of the above requirements, designing of larger ligands to obtain larger pore apertures has been challenging as this may result in interpenetrated networks (**Figure 1c**). The inherent structure of MOFs contain pathways which allow easy diffusion of ionic species but there exist some fundamental issues which should be addressed before the efficient use of MOFs. The crystalline structure of MOFs could be an advantage in several applications but a less packed solid would provide better transport of the ionic species during electrochemical reactions. Also, a network with functional groups along the MOF chains is preferred for enhanced conduction properties. Very recently, a Zn-based MOF interconnected with 1,2,4-trizole and orthophosphates was developed to demonstrate intrinsic proton conduction as shown in **Figure 1d**.[63] A 2D layered structure with extended networks of hydrogen bonds between the layers provide excellent pathway for conduction.

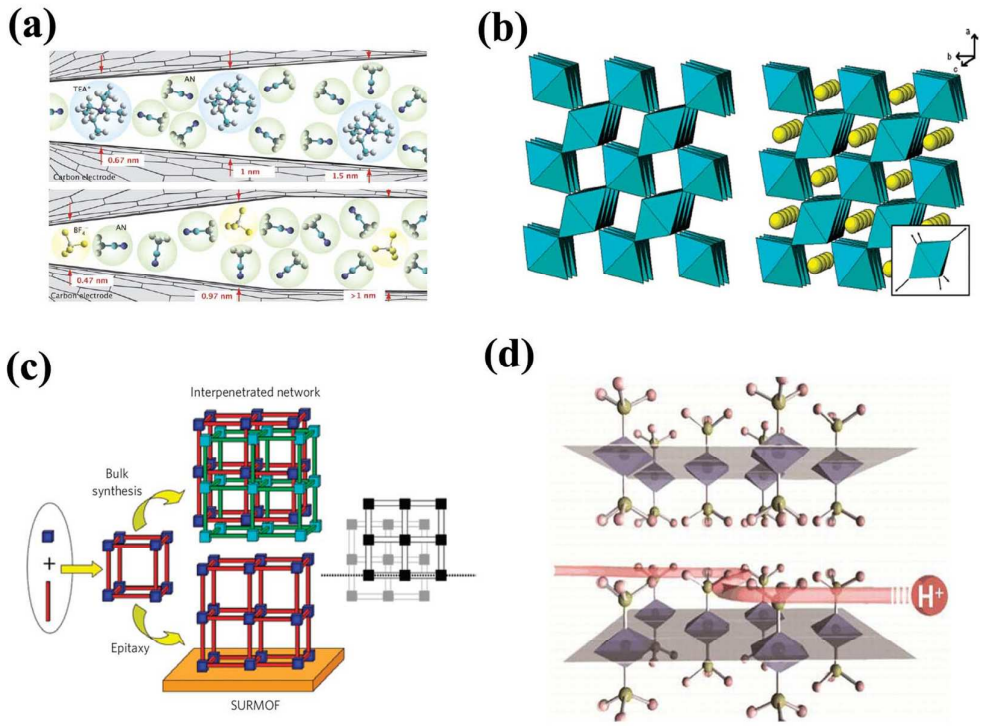

Figure 1. (a) Geometric confinement of ions in extremely small pores. Both anions and cations enter the pores with no solvent-molecule screening charge at pore sizes below 1.5 and 1 nm, respectively. Therefore, it can be asserted that the ions enter the pores either bare or with partial solvent shells (TEA^+ = tetraethylammonium, AN = acetonitrile).[61] Reproduced with permission of Wiley-VCH Verlag GmbH & Co. KGaA. (b) Crystal structures of MnO_2 and Li_xMnO_2 viewed down the 1 × 1 tunnels. Inset shows the distortion of the MnO_6 octahedra on intercalation of Li^+.[62] Reproduced with permission of American Chemical Society. (c) Representation of MOF synthesis concepts. Using conventional synthesis, often two equivalent networks (colored red and green) are formed at the same time. Using liquid-phase epitaxy, the equivalence of these two networks is lifted by the presence of the substrate (dotted line in the schematic diagram on the right) and the formation of interpenetrated networks is suppressed, yielding SURMOFs containing only one network.[7] Reproduced with permission of Nature Publishing Group. (d) Inherent proton conduction in MOF.[63] Reproduced with permission of American Chemical Society.

MOFs, owing to their unique composition and topology, have been widely used as sacrificial templates to produce high surface area and ordered nanostructured materials including carbon, MOs, MO@C, and M@C composites for electrochemical applications. The MOF derived materials possess unique advantages of controlled porosity, higher activated surface areas and ease of synthesis. The surface area and

pore size of the carbon products strongly depend on the starting MOF precursors. Very recently, the effect of ligands towards the properties of resulting carbon was explored.[64] It was demonstrated that using highly porous MOF could lead to carbons with higher surface areas as compared to nonporous MOF derived carbon which possess relatively lesser surface area (**Figure 2a)**.[65]

It has also been demonstrated that electrolyte could only diffuse up to a maximum thickness of 20 nm in a bulk crystalline material while most of the bulk electrode materials have thicknesses of more than 20 nm.[66,67] This puts forward a need to develop materials with minimal thicknesses and high active surface area. MOFs provide the opportunity to synthesize high surface area MO nanostructures including hollow structures (containing single MO or multi MOs with hollow core-shell structures) by simple thermal treatment, which have been considered as very promising in the field of electrochemical applications. A simple method was generalized to tailor the multi-shell hollow MO nanostructures (Fe_2O_3/M_xO_y) from MOFs with high surface areas **(Figure 2b)**.[68] It is quite clear that MOF derived structures strongly depend on the starting properties of MOF precursors, which leads to the fact that a thorough understanding of MOFs and the targeted properties/application could lead to very promising results rather than using hit and trials methods.

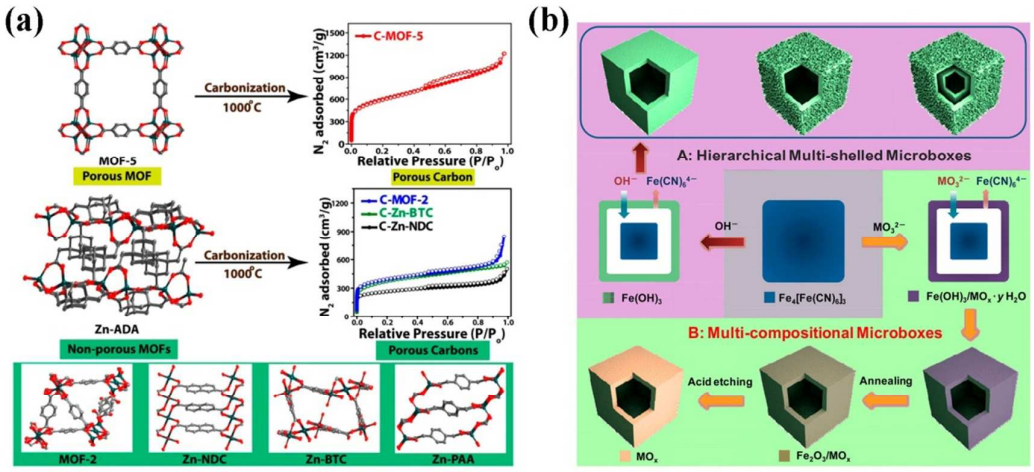

Figure 2. (a) Schematic representation for the synthesis of porous carbon on direct carbonization of porous and nonporous MOFs at 1000 °C along with their N_2 adsorption isotherms.[65] Reproduced with permission of American Chemical Society. (b) Schematic illustration of the formation of hierarchical multi-shelled (route A) and multi-compositional (route B) metal oxides microboxes starting with metal-organic frameworks templates. Metal oxides microboxes were synthesized by manipulating the ion exchange reaction between a proper alkaline precursor (strong base or conjugate base of the weak acid) and a sacrificial PB by the following reactions. Route A: $12OH^{-}$ (aq) + $Fe_4[Fe(CN)_6]_3$ (s) → $3Fe(CN)_6^{4-}$ (aq) + $4Fe(OH)_3$(s). Route B (for the case Sn): $6SnO_3^{2-}$ (aq) + $Fe_4[Fe(CN)_6]_3$(s) + $6(1 + x)H_2O$ → $3Fe(CN)_6^{4-}$ (aq) + $4Fe(OH)_3$(s) + 6 $SnO_2 \cdot xH_2O$(s).[68] Reproduced with permission of American Chemical Society.

3. Derivation of various structures from MOFs

Carefully controlled micro- and mesoporous nanostructured materials are expected to act as clean sources to overcome the energy requirements of the recent times. Apart from using pure MOFs for electrochemical applications, using MOFs as sacrificial materials to obtain highly controlled nanostructured materials has increased tremendous attention in recent years.[29] A number of reports have been published recently demonstrating superiority of MOF derived materials for electrochemical energy storage over other materials synthesized by traditional methods.[69,70] The use of MOFs to develop nanostructured materials has been boosted by the fact that MOF are

highly porous, crystalline materials which could be converted to desired product by one step calcination process which enhance their practical application at pilot and industrial scale.[71,72] Due to these advantages, MOF materials have been successfully used to develop nanostructured carbon,[73] MOs,[74] composites (M/MO@C)[75] and nanoparticle decorated MOFs.[76] In this section, we will review the major methodologies used for derivation of these nanostructures.

3.1 Carbons

Nanoporous carbon has attracted wide attention of scientific community for electrochemical energy storage due to the abundant resources and excellent thermal and chemical stability. Careful control on carbonaceous nanostructures not only boost up the capacitive energy storage but also provide an opportunity to tailor materials for high rate reversible intercalation of Li^+ ions in LIBs. Moreover, high surface area carbons have also been widely used to fabricate other highly efficient redox active nanostructures for energy storage, which further demonstrate its importance. In essence, it is very important to develop novel techniques/methods that could help in tailoring the porosity and morphology of the carbonaceous nanostructures. Intense struggle in past 20-30 years to control carbon nanostructures has led to various characteristic structures but the field is still in growing phase. Different materials have been introduced to develop highly ordered nanoporous carbon by using complicated processing condition. Owing to the high surface area and defined structure, MOFs present excellent sources for derivation of carbonaceous materials with desired inherent properties. Since MOFs are constructed from the combination of inorganic

metallic species with organic moieties, decomposition of MOFs at higher temperature under different conditions could generate a large variety of products from porous carbon to metal oxides, metal sulfide, metal carbide, metal and metal oxide decorated carbon composites.

Carbon can be derived from MOFs by carbonization in several ways with or without post treatment. Since MOFs inherently consist of metallic species which are integral part of the whole structure, it is essential to remove these metallic species to get high surface area carbon. An efficient approach in this conquest was first introduced by us through the usage of Zn-based MOFs to derive carbon materials.[77] This process introduced simultaneous carbonization process along with decomposition of MOF and removal of metallic species. We suggest decomposition of MOF precursor upon thermal treatment in inert atmosphere where Zn is converted to ZnO upon structural disintegration. ZnO has the very high boiling point (2360 °C) compared to Zn (908 °C), so it is difficult to remove ZnO at relatively lower temperatures (900-950 °C). However, the decomposition of MOF results in formation of carbon as well, which can effectively reduce ZnO into Zn at 900 °C resulting in evaporation of Zn at these temperatures leaving behind highly porous carbon. This carbon synthesis method from MOFs has been reported by several groups[77,78] and is efficient for Zn-based MOFs at relatively high carbonization temperatures. On the other hand, at lower carbonization temperatures or in case of MOFs consisting of other metals with higher boiling points than Zn (such as Fe, Co, Cu, etc.), carbonized

samples could retain the metallic species. It will generate extremely porous carbon products after post acid wash treatment (**Figure 3**).[79]

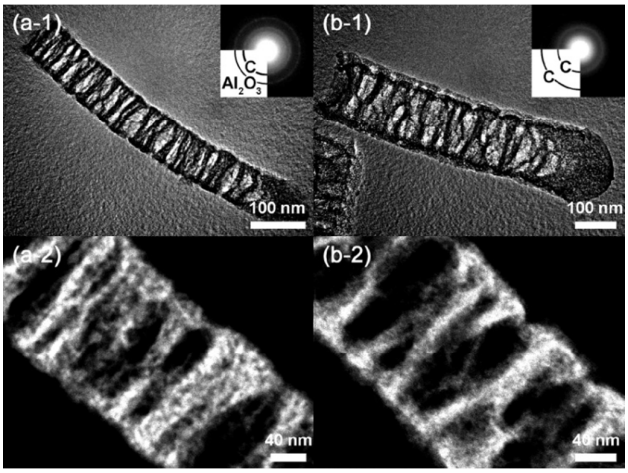

Figure 3. Bright- and dark-field TEM images of Al-PCP calcined at 800 °C (a) before and (b) after washing with HF. The inset is the corresponding ED pattern.[79] Reproduced with permission of American Chemical Society.

Since MOFs consist of large cavities, a secondary source can be infiltrated in these cavities in order to improve the characteristics of the resulting product such as surface area and porosity. After the initial work of using pristine MOFs to obtain high surface area carbon, we introduced furfuryl alcohol (FA) as secondary carbon source into MOF to obtain unexpectedly high surface areas (3405 m^2/g) and pore volumes (2.58 cm^3/g).[80] Carbonization of MOF without any secondary precursors commonly results in low surface area carbonaceous materials, which have been addressed by post treatment of the carbonized product. Heating a mixture of carbonized product with potassium hydroxide (KOH) at high temperatures followed by acid washing to remove impurities commonly result in high surface area carbons (>2000 m^2/g).[81,82] Although all the MOFs were treated through the same way, it was difficult to

underline the difference in surface areas of carbons synthesized from various MOFs, which will be explained in next section.

It is assumed that heating rate, carbonization time and MOF ligands play critical role in resulting carbonaceous materials. Many studies reported the synthesis of nanoporous carbon,[83-86] but most failed to account for insights into carbonization process, which however has been addressed recently.[87] **Figure 4** shows two-step carbonization process of isoreticular MOFs (IRMOFs) at 550 °C and 900 °C together with the XRD and optical spectra of the products. Effect of temperature upon direct carbonization of several Zn-based IRMOF has been studied to optimize the structure of nanoporous carbons. This work suggests better control over porosity of MOF-derived carbon by careful selection of MOF precursor. Authors demonstrated further insights into the carbonization process by using the temperature-programmed desorption (TPD)-mass spectroscopy. The MOFs were converted into metal oxide/carbon composite at lower temperatures (< 750 °C) upon degradation of the main MOF structure while increase in temperature led to formation of pure carbonaceous material at 900 °C. The complete removal of Zn species at such low temperature was attributed to the reduction of ZnO to Zn by carbon between 750-900 °C. Subsequent vaporization of Zn species led to formation of pure carbonaceous product with high surface area of 3447 m^2/g.

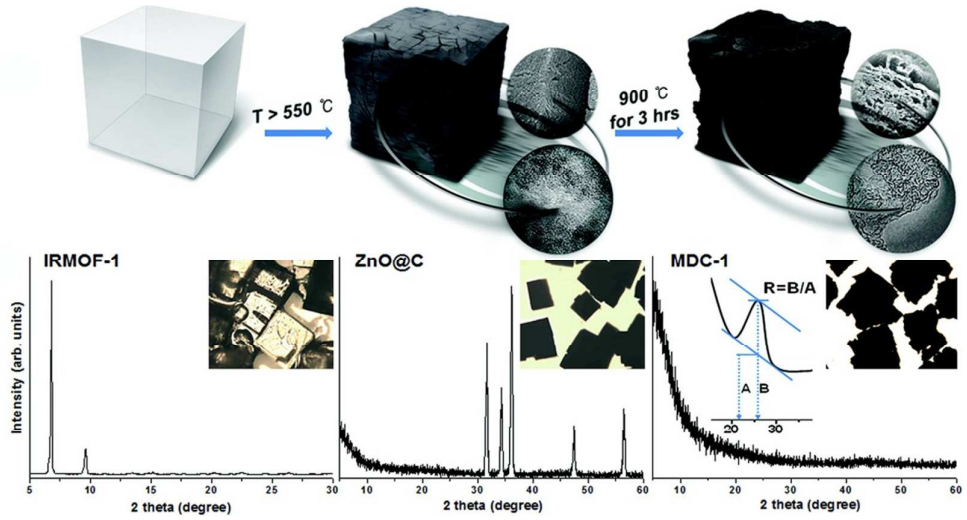

Figure 4. Structural changes of IRMOF-1 with heat-treatment to yield MDC-1: schematic view (up) and PXRD patterns with corresponding optical micrographs (down).[87] Reproduced with permission of American Chemical Society.

Several methods have been demonstrated for successful derivation of high surface area carbons, but very few reports could grasp the effect of versatility of MOFs upon the properties of the resulting carbon. MOFs could be synthesized with different types of organic ligands resulting in various cavity types, so it is important to develop a general understanding towards the carbonization process. The importance of choosing proper MOF for targeted applications was demonstrated recently by researchers who synthesized various MOFs with decreasing aromaticity to explore the effect to the products.[65] Several Zn based MOFs (e.g. MOF-2, MOF-5, Zn-BTC) were chosen as representative MOFs**.** The work clearly demonstrated a decrease in surface area with decreasing aromaticity in the starting framework. MOF-5 with the highest aromaticity provided carbon product with the highest surface areas. To obtain high

surface area carbon without post treatment, MOF precursors with high surface area and high aromaticity is preferable.

It is fascinating to find that the diverse MOFs enable multi forms of carbon products ranging from zero- to three-dimension. We first introduce the strategy to construct zero-dimensional carbon from MOFs. Specifically, ZIF-8 nanoparticles were first prepared with ultrasonication and heated at a mild temperature (500 °C), which gave carbon nanodots with an average particle size of 2.2 nm (**Figure 5a**).[88] Carbon nanotubes, a typical one dimensional material, can be prepared from MOFs with metal species like Fe, Co, Ni. During high temperature treatment process, metallic Fe, Co or Ni nanoparticles are first formed and catalyze carbon nanotube formation on the surface. A Ni-MOF, $Ni_3(btc)_2 \cdot 12H_2O$ (btc = benzene-1,3,5-tricarboxylate), was pyrolyzed in a conventional tube furnace under 500 °C for 20 h, which resulted in multiwalled carbon nanotubes without any additional catalyst or carrier gas (**Figure 5b**).[89] Two dimensional carbon materials can also be prepared from MOFs.[90] A ZIF-7/glucose composite was carbonized under an Ar atmosphere at 950 °C for 5 h and graphene-like carbon nanosheets were obtained (**Figure 5c**). It was found that the addition of glucose as carbon source was important for the formation of graphene-like structures, attributing to the pre-melting and polymerization of glucose before complete ZIF-7 carbonization. We extended the morphology of MOF-derived materials to three-dimensional nanostructure.[81] Al-BTC metal-organic aerogels were constructed from a simple mixture of aluminum nitrate and 1,3,5-benzentricarboxylic acid and followed supercritical CO_2 drying process.

The aerogel was then converted into three-dimensional carbon after carbonization and purification (**Figure 5d**). The obtained samples showed hierarchically porous structure and high surface area (1820 m^2/g). These examples demonstrate the versatility of MOF and MOF-derived carbon products. The successful structure evolution from MOFs could enable various applications of the derived materials based on the structure characters, which will be discussed in next parts.

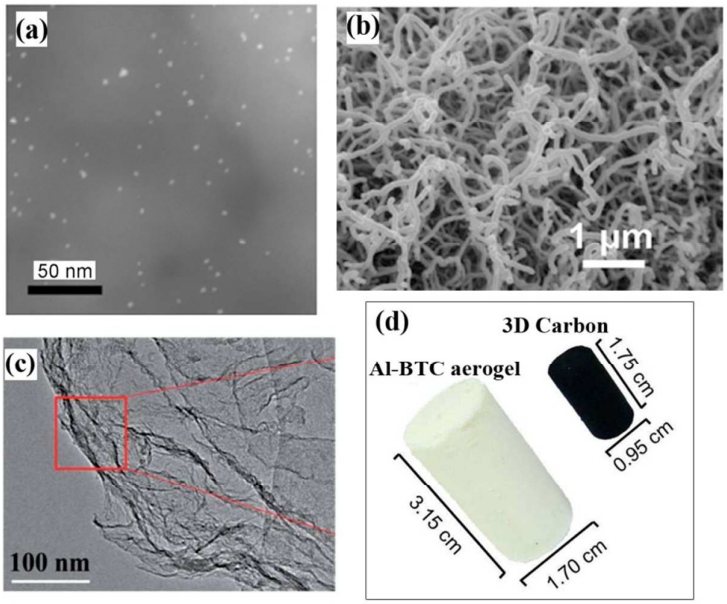

Figure 5. MOF-derived 0D to 3D carbon materials. (a) HAADF-STEM image of ZIF-8 derived quantum-sized carbon nanodots.[88] (b) SEM image of Ni-MOF derived multi-walled carbon nanotubes.[89] Reproduced with permission of Royal Society of Chemistry. (c) HRTEM image of ZIF-7 derived graphene-like carbon nanosheets.[90] Reproduced with permission of Royal Society of Chemistry. (d) Photograph of an integrate Al-BTC aerogel and its derived 3D carbon.[81]

3.2 Metal Oxides

Synthesis of nanostructured metal oxides (MO) for electrochemical applications has been under intense investigation with particular interest in controlling shape, size, composition, porosity and surface area of the resulting MOs. Different chemical and

physical methods have been proposed to develop MOs but their practical application is still limited due to the complicated process which are difficult to generalize at pilot scale. In this regard, MOF pyrolysis strategy has emerged to be promising candidate providing opportunity to tailor MO structures in several ways and develop large scale production fulfilling industrial needs. Owing to the inherent structure of MOFs, which is made of metal centers coordinated with organic complexes, controlled heating in various environments can provide unique structures with tailorable porosity. A successful derivation of high surface area MOs (Fe_2O_3~200-400 m^2/g) from Prussian Blue, $Fe_4[Fe(CN)_6]_3$, was reported.[91] It was demonstrated that surface areas of the resulting MOs strongly depend on the size of the MOF particles. The increase in MOF particle size effectively resulted in the decreased surface area of the resulting MO nanostructures. Despite this initial report, there has been a slow progress in the derivation of MOs from MOFs. It was not until very recently that many research progresses were reported. In 2010, we reported a Co-MOF derived Co_3O_4 particles with a size of about 25 nm; however it has a low surface area of 5.3 m^2/g.[92] Several metals could have different oxidation states depending upon the calcination conditions (e.g. Fe_2O_3 and Fe_3O_4). A selective conversion of MIL-88b to generate either Fe_2O_3 or Fe_3O_4 rods was demonstrated.[93] The authors demonstrated that calcination in air could only provide hematite (α-Fe_2O_3) via direct thermal conversion of MIL-88b while a two-step method (calcination followed by heating in inert atmosphere) provided the magnetite (Fe_3O_4) as shown in **Figure 6a.**

For improved electrochemical performance, a better control over the MO structure is highly appreciated. For example, a high surface area MO nanostructure could provide more sites for intercalation of Li^+ ions in case of LIBs, while a large number of redox sites would be available for supercapacitors. Similarly, flux of electrolyte at higher rates could be lone capacity determining factor even if the material has high surface area, which makes the suitable pore size in MO nanostructures a very critical factor. A new idea was introduced in tailoring the MO nanostructures by using a two-step thermolysis method including carbonization in N_2 environment and oxidation in air.[94] Using MIL-88(Fe) as sacrificial template, spindle like mesoporous structures of Fe_2O_3 with a surface area of 75 m^2/g were obtained (**Figure 6b)**. Microstructure analysis show that the product is highly porous and consist of uniform nanoparticles with a size of about 20 nm. The authors also compared the two step synthesis method with direct oxidation of MIL-88 and demonstrate its superiority over one step oxidation which resulted in much lower surface area product.

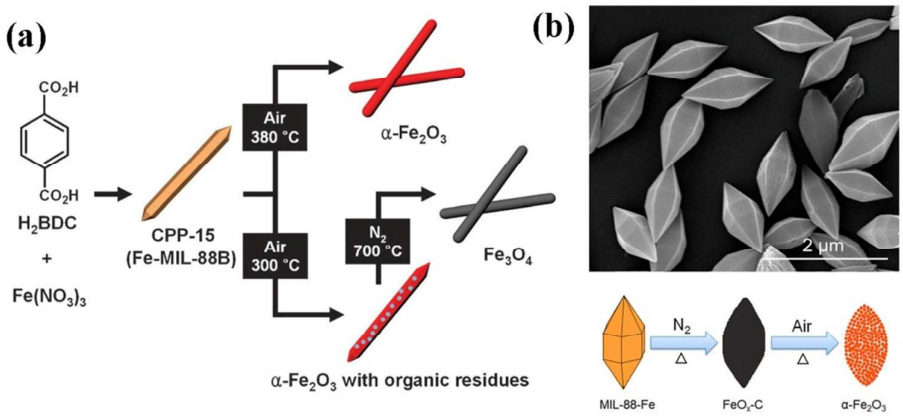

Figure 6. (a) The selective preparation of hematite (a-Fe_2O_3) and magnetite (Fe_3O_4) nanorods from coordination polymer nanorods (CPP-15).[93] Reproduced with permission of Royal Society of

Chemistry. (b) SEM image of as-prepared MIL-88-Fe (up) and illustration of the fabrication of spindle-like porous α-Fe_2O_3 (down).[94] Reproduced with permission of American Chemical Society.

A major drawback in practical application of MOs at industrial scale is the poor cyclic behavior due to material deterioration. MOs react reversibly with lithium (Li) ions (in case of Li-ion batteries) during charge/discharge process which leads to volumetric changes in the electrode materials. It is highly desirable to develop materials which can offer some free space to accommodate these volumetric changes. Growth of well-controlled and desired hierarchical hollow nanostructures has been identified as a possible solution to this emerging issue. Hollow structures could offer higher surface areas, free void spaces to accommodate volumetric changes, very low density and relatively high loading capacity, which have been highly desirable for advancement in electrochemical energy storage. Several interesting approaches including Kirkendall effect, galvanic replacement, chemical etching, thermal decomposition and self-templating have been developed to obtain the hollow structures.[95] Owing to the preformed network in the framework, MOFs could be converted into well controlled, highly porous hollow MO nanostructures. Fe_2O_3 microboxes with hierarchical shells were developed by utilizing simultaneous oxidative decomposition of Prussian Blue (PB) microcubes (**Figure 7**).[96] It was demonstrated that the thermolytic temperature plays critical role in defining the shape of resultant product. For instance, Fe_2O_3 microboxes were obtained when PB was decomposed at 350 °C. When the temperature was increased to 550 °C, porous Fe_2O_3

microboxes were obtained. Further increase in temperature to 650 °C resulted in the hierarchical microboxes containing Fe_2O_3 nanoplatelets.

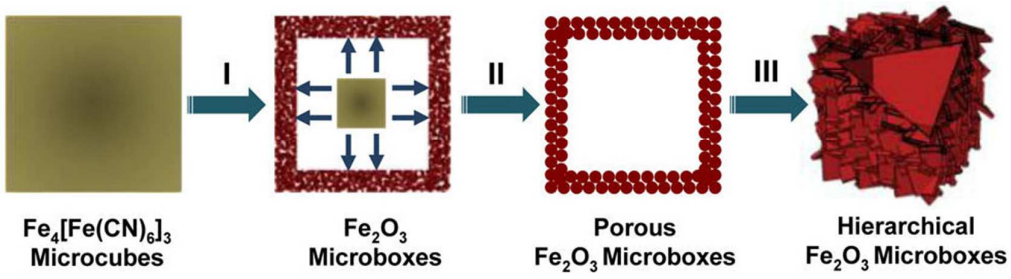

Figure 7. Schematic illustration of the formation of hollow Fe_2O_3 microboxes and the evolution of the shell structure with the increasing calcination temperature.[96] Reproduced with permission of American Chemical Society.

MOF-based MOs provide another unique feature in material fabrication by allowing the existence of multiple metallic species in the same framework. Mixed metal oxides (general formula AB_2O_4) have got tremendous interest recently due to complex chemical compositions, improved electrical, chemical and magnetic properties that induced by the synergistic effect of various metallic species and presence of multiple valences of contributing metals, but controlled synthesis of these materials remains a big challenge.[97] MOF-derived mixed metal oxides have shown considerable electrochemical activities owing to their high surface area (improving interfacial area between electrode/electrolyte), and flexibility in composition modification. Recently, spinel $ZnMn_2O_4$ and $NiMn_2O_4$ nanoplates assemblies were prepared from MOF precursors through an "escape by crafty scheme" strategy (**Figure 8a**).[98] Heat treatment temperature was identified to be critical for obtaining the desired spinal MOs. Although thermolysis of MOFs at relatively lower

temperatures could give MOs, spinal structures can only be obtained at relatively high temperatures. Mixed valence metal oxides hollow structures have been prepared from MOFs recently by thermolysis at 350 °C, as shown in **Figure 8b**.[99] It was demonstrated that the synthesized mixed valence (CuO/Cu_2O) nanostructures could provide superior performance as anode materials in LIBs (740 mAh/g at 100 mA/g).

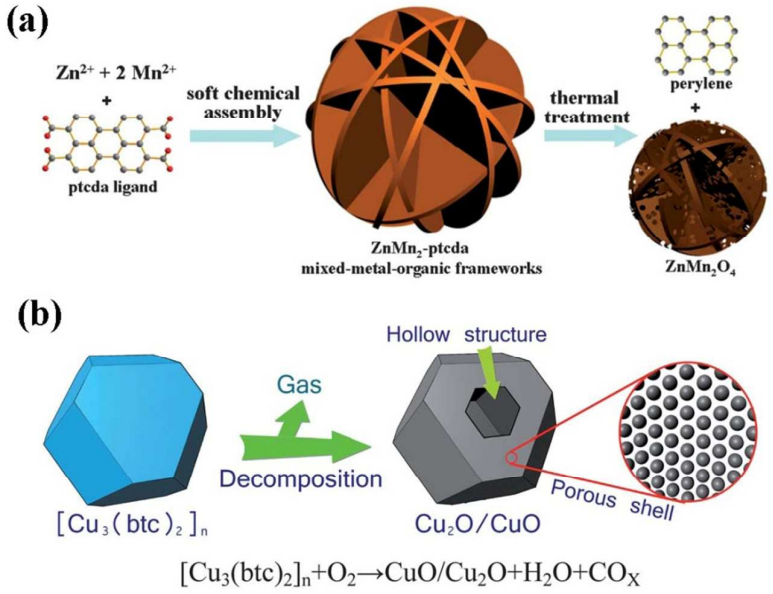

Figure 8. (a) Illustration of the two step process for the preparation of spinel $ZnMn_2O_4$ using $ZnMn_2$–ptcda as a precursor by an ''escape-by-crafty-scheme'' strategy.[98] Reproduced with permission of Royal Society of Chemistry. (b) Schematic illustration of the formation of CuO/Cu_2O hollow polyhedrons with a porous shell.[99] Reproduced with permission of Royal Society of Chemistry.

The onus of recent researches has been concentrated on developing core-shell structures for superior electrochemical properties. Several MOFs have been developed with core-shell structures for various applications, but deriving core-shell MO nanostructures from MOFs has been challenging. It is widely believed in the light of recent literature that core-shell redox active species could provide superior Li^+ storage

capacity while maintaining reversibility at higher scan rates, however the practical application of such structures is primarily limited due to lack of flexibility that lead to decomposition upon formation of SEI layers. Along with the core-shell structures, a major design requirement for practical application of nanostructures in LIBs is the inherent presence of voids which can accommodate volume changes during cyclic testing. Very recently, a thermal conversion of $Co_3[Fe(CN)_6]_2$@$Ni_3[Co(CN)_6]_2$ nanocubes to porous Fe_2O_3@$NiCo_2O_4$ nanocages was demonstrated.[100] Firstly, NiCo was used as a core to grow FeCo on its surface. Then the FeCo@NiCo sample was annealed at 450 °C, which provided a core-shell oxide nanostructure of Fe_2O_3@$NiCo_2O_4$. It can be seen clearly in **Figure 9** that the core of the oxide particle is hollow while Fe, Co and Ni are well-distributed on the edges. This interesting structure can efficiently tune the stress, alleviate the pulverization effect, and thus enables the good rate capability and cycling performance.

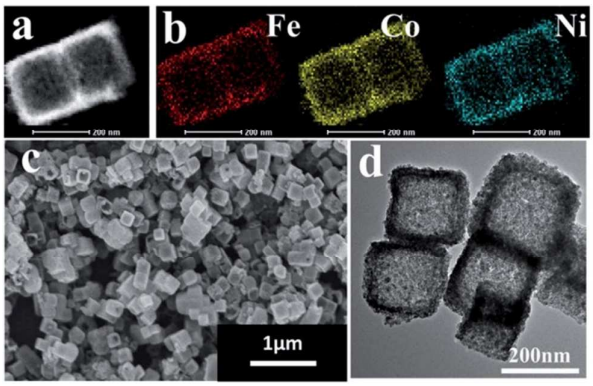

Figure 9. (a) HAADF-STEM image, (b) elemental mappings, (c) SEM image and (d) TEM image of Fe_2O_3@$NiCo_2O_4$ nanocages.[100] Reproduced with permission of Royal Society of Chemistry.

3.3 Metal Oxide/Carbon Composite

Although MOs can provide high capacity for electrochemical energy storage, they lack stability due to large volume expansion during charge/discharge process. Several advancements have proved that the use of secondary species can uphold these volumetric changes while retaining the inherent high electrochemical performance. Nanoporous carbonaceous matrix with high surface area has been identified as a stabilizer in charge/discharge process. Synthesizing MO/C composites by traditional chemical synthesis methods leads to poor control over MO particles sizes due to agglomeration that would severely affect the performance of the electrode materials. Surface coating has also been considered as a promising method for limiting particle agglomeration while retaining high performance. Since MOFs can generate high surface area carbon upon heating, thermolysis can be optimized to obtain highly porous MO/C, M/C, and MC/C composites.[101] An excellent report recently emphasized the successful derivation of 3-D carbon decorated with ultra-small (3.5 nm) ZnO quantum dots from IRMOFs by controlled heat treatment (**Figure 10)**.[102] As discussed earlier, the particular advantage of using MOF templates to derive MO/C over traditional synthesis methods was the production of the carbon coated MO particles with uniform dispersion. In continuation to previous progress, carbonization temperature was again found to be a key factor along with duration of heating and heating rate. An increase in carbonization temperature quickly led to irregular particles (20 nm) and loss of original structure. Although MO/C nanostructures commonly exhibit very low surface areas, the synthesized ZnO/C exhibit a high surface area of 513 m^2/g and a large pore volume of 1.27 cm^3/g due to the inherent

pore retention. The method provided a general approach towards successful synthesis of MO@C nanostructure for highly efficient electrode materials.

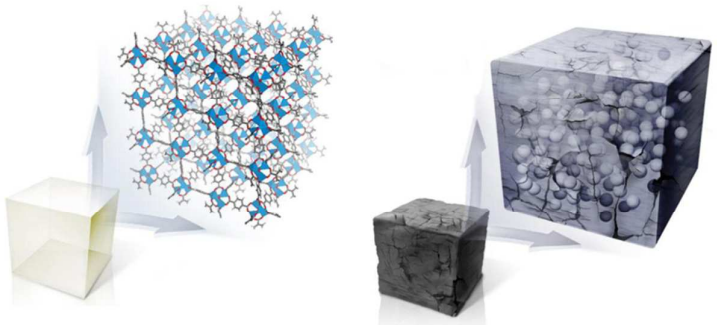

Figure 10. Schematic diagrams of IRMOF-1 (left) and IRMOF-1 after controlled pyrolysis to produce carbon-coated ZnO QDs without agglomeration (right). The ZnO QDs are covered with a thin amorphous carbon layer that acts as a buffer layer to confine the QDs during the charging and discharging steps.[102] Reproduced with permission of American Chemical Society.

Subsequent works reported the optimization of carbonization process to rationally obtain metal (M) or MO particles. An important study in this regard came from researchers who defined the limits to obtain M, MO and mixed M/MO particles from MOF.[103] The authors used several MOFs (MOF-4, Co-HFMOF-D, Zn-ADA-1, Mn-HFMOF-D, Cd-MOF-1, MOF-CJ4, HKUST-1) based on different metals (Zn, Mn, Cd, Co, Cu and Mg) to derive several M/MO@C composites at the same carbonization temperature of 900 °C. It was concluded that reduction potential play critical role in determining the resultant product. If the reduction potential of the coordinating metal is -0.27 or higher, carbonization process would produce metallic species upon thermolysis. However, if the potential is lower than -0.27, thermolysis would lead to formation of MO in the product (**Figure 11)**. **Table1** summarize the different type of species (M or MO) formed under different carbonization conditions.

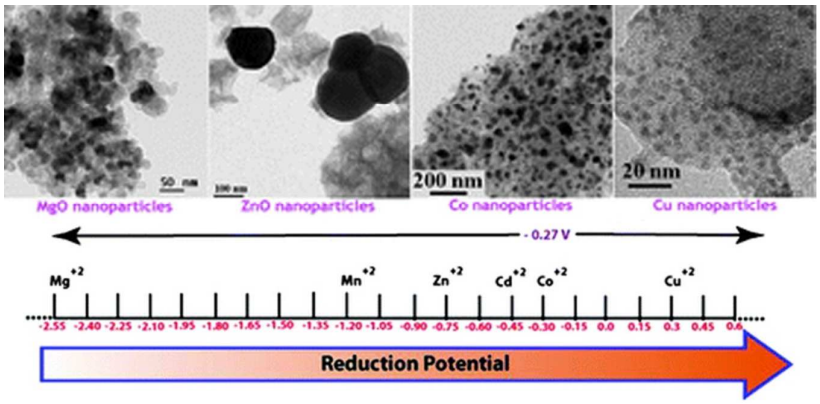

Figure 11. The effect of reduction potential of metal atoms present in the MOFs on the formation of the metal/metal oxide nanoparticles. Metals having a reduction potential above -0.27 V undergo thermolysis in an N_2 atmosphere to give pure metal nanoparticles, whereas metals with reduction potential less than -0.27 V, even in an N_2 atmosphere, produces metal oxides only.[103] Reproduced with permission of Royal Society of Chemistry.

Table 1. Formation of the M/MO nanoparticles from their corresponding MOFs in air and nitrogen atmospheres during pyrolysis.[99]

MOF Type	Atmosphere during thermolysis	
	Nitrogen	Air
$[Cu_2(hfbba)_2(3\text{-mepy})_2](DMF)_2(3\text{-mepy})$	Cu nanoparticles	CuO nanoparticles
$[Co_2(hfbba)_2(3\text{-mepy})_2](DMF)_3$	Co nanoparticles	Co_3O_4 nanoparticles
$[Zn(ADA)(4,4'\text{-bipy})_{0.5}]$	ZnO nanoparticles	ZnO nanoparticles
$Mg_3(O_2CH)_6[NH(CH_3)_2]_{0.5}$	MgO nanoparticles	MgO nanoparticles
$[Cd(ADA)((4,4'\text{-bipy})_{0.5})]DMF$	CdO nanoparticles	CdO nanoparticles
$[Mn_2(hfbba)_2(3\text{-mepy})](H_2O)$	——	Mn_2O_3 nanoparticles
$[Cd(tdc)(bpy)(H_2O)]_n$	CdS nanoparticles	CdO nanoparticles

3.4 Metal-Nanoparticles@MOFs

Owing to the presence of active sites and high surface area, MOFs have been widely studied for catalytic reactions in organic and electrochemistry. Although pristine

MOFs show considerable activity towards catalysis, recent progress is more focused on decorating MOF scaffolds with precious and non-precious active nanoparticles for electrochemical applications. A number of active materials such as Pt,[104] Pd,[105] Ru,[106] Au,[107] Ag,[108] Cu,[109] Ni,[110] Mg[111] and active bimetallic nanoparticles such as Pt-Pd,[112] Pt-Ru,[113] Pt-Ni,[114] Pd-Cu,[115] Au-Pd,[116] Au-Ag,[117] Au-Co,[118] Au-Ni[119] and Cu-Co[120] have been successfully decorated in MOFs. Several methods have been proposed to obtain M@MOF structures including incipient wetness impregnation, solid grinding, microwave assisted growth, gas phase infiltration, *etc*.[121] Some excellent reviews have addressed recent research progress and challenges in this field.[121-126] A recent breakthrough gives insight into the successful incorporation of M/MO nanoparticles (mono- and bimetal) into MOF structures by taking into account the reactivity of organic-inorganic moieties during MOF synthesis (**Figure 12**).[127] Such encapsulation method has been generalized for decorating several types of nanoparticles, imparting specified functionalities to the MOFs.

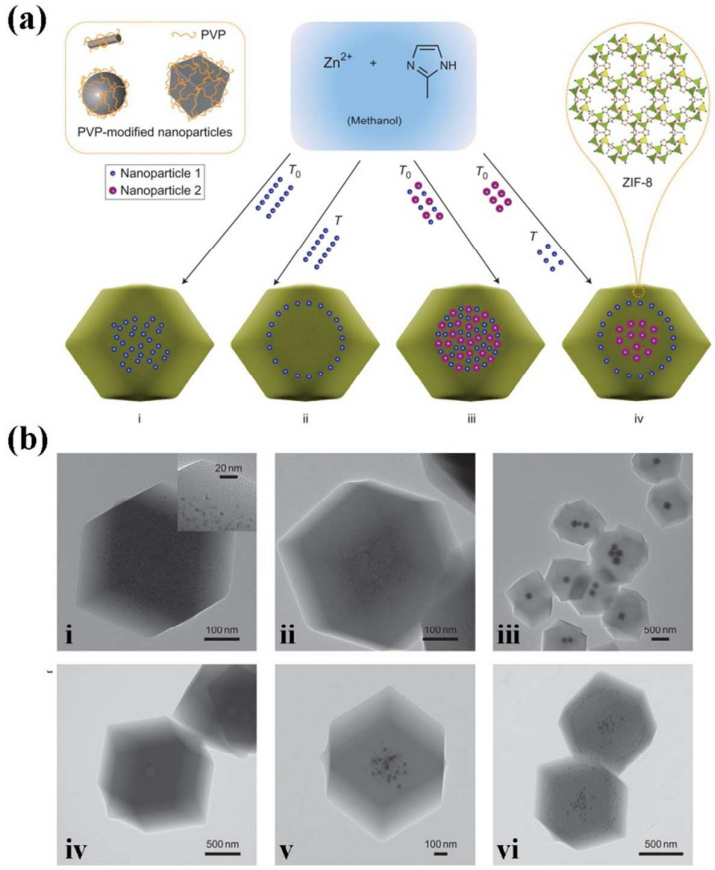

Figure 12. (a) Scheme of the controlled encapsulation of nanoparticles in ZIF-8 crystals. (b) TEM images of nanoparticle/ZIF-8 composites that contain different types of nanoparticles. i, ii, Hybrid crystals that contain 3.3 nm Pt nanoparticles with Pt contents of 3.4% (i) (inset: high magnification image) and 0.7% (ii), respectively. iii, Hybrid crystals that contain Ag cubes (of average size 160 nm). iv, Hybrid crystals that contain 180 nm PVP-modified PS spheres with surfaces that were partially coated with unmodified 13 nm Au nanoparticles. v, Hybrid crystal that contains homogeneously distributed 13 nm Au and 34 nm Au nanoparticles in the central area. vi, Hybrid crystals that consist of 34 nm Au nanoparticle-rich cores, 13 nm Au nanoparticle-rich transition layers and nanoparticle-free shells.[127] Reproduced with permission of Nature Publishing Group.

Although several loading techniques were demonstrated earlier, it was not until very recently that a quantitative technique was defined. Taking into account the total available space in MOFs to accommodate maximum amount of nanoparticles, we introduced a post synthesis double solvent (organic-inorganic) technique for

complete encapsulation of nanoparticles inside MOFs without agglomeration on the outer surface (**Figure 13a**).[128] Cr-based MOF (MIL-101) with hydrophilic zeotypic cavities was selected. A mixture of hexane (hydrophobic) and water (hydrophilic) carries the M^{+} (Pt^{4+}) into the MOF cavities followed by reduction of M^{+} (Pt^{4+}) to obtain M (Pt) nanoparticles decorated MOF. This method has also been further generalized by fabricating mono- and bimetallic species in the MOF structures (**Figure 13b**).

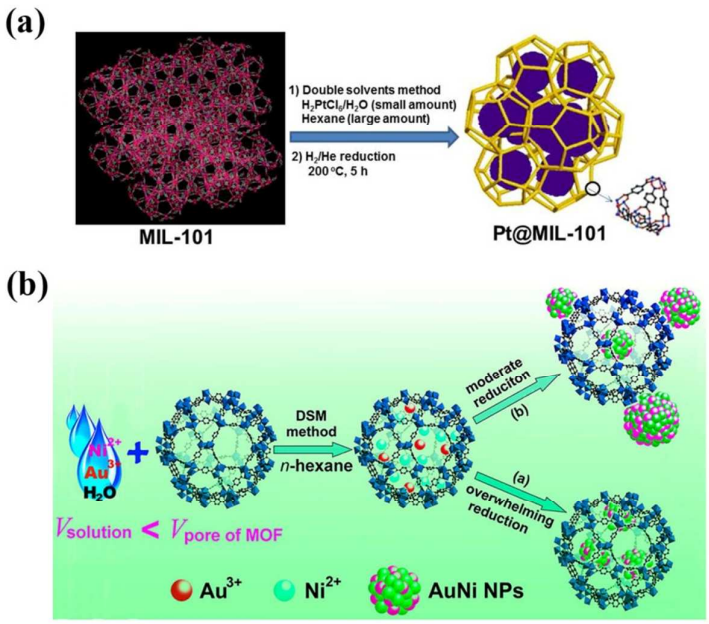

Figure 13. (a) Schematic representation of synthesis of Pt nanoparticles inside the MIL-101 matrix using double solvents method.[128] (b) Schematic representation of immobilization of the AuNi nanoparticles by the MIL-101 matrix using the double solvents method combined with a liquid-phase concentration-controlled reduction strategy.[119]

4. Electrochemical Energy Storage Applications

Electrochemical energy storage has been considered to be the most promising form of energy storage and energy production in recent times, and it is expected to take over

the traditional gasoline industry in near future to light up small portable devices to large vehicles. Since the introduction of LIBs in the commercial market, there has been increased research interest to address the looming issues in this field. Despite several improvements, these advancements are always limited by several issues including low utilization, electrode pulverization and relatively low electrochemical activity. Recently MOFs have provided a breakthrough in this field as they possess high surface area frameworks which can incorporate nanostructured active species to exploit the full potential of the materials. The extremely low densities of MOFs provide good opportunity to load large amount of active nanostructured species into the framework, which is not possible in other developed support materials. Here we will summarize recent progress in this field and demonstrate potential improvements which can lead to ultimate success of these materials.

4.1 Supercapacitors

Supercapacitors provide a quick way of energy storage with fast charge/discharge rates thus giving very high power densities. Traditional supercapacitors known as electrochemical double layer capacitors (EDLC) store energy by the formation of an ionic double layer which diffused very quickly providing very fast discharge, consequently giving higher power densities. The most important parameters which influence/determine the capacitive performance of EDLC are surface area, pore size distribution, pore volume and size of the electrolyte ions in solvated and desolvated shells.[129-132] Another important class of supercapacitors includes redox active species

employing a reversible Faradaic reaction to store charges (named as pseudocapacitors).[133-135] This class of materials has shown considerably high capacitance capabilities improving the energy densities by at least an order of magnitude. The pseudocapacitance of the materials strongly depends on the size of the redox active species, porosity (to allow fast access of the electrolyte), crystallinity (optimizing the deep diffusion of the electrolyte) and surface area of the electrode materials. Owing to the presence of both metallic and organic moieties, MOFs present novel synthetic materials consisting of inherently high surface areas and well-defined pore size distribution with both redox active species and surfaces for double layer formation. Several pristine MOFs have been investigated for capacitive energy storage.[136,137] The use of pristine MOF for supercapacitive charge storage was demonstrated by researchers who successfully employed some Ni-based MOFs.[137] Since this MOF consisted of Ni, reversible CV scan of the pristine MOF provided evidence of reversible redox reaction from coordinated Ni, which gave high capacitance value up to 634 F/g. MOFs can have various topologies with multiple organic ligands, different metal ions, varying pore sizes, discrete metal oxide backbones, various sizes of nanocrystals and different shapes, it is important to assemble the work together at one place. Very recently, a wide range of pristine MOFs (MOF-5, MOF-74, HKUST-1, ZIF-8, MOF-801, UiO-66, UiO-67, MOF-177, MOF-808 and MOF-867) was explored for supercapacitive energy storage.[138] A series of 23 MOFs synthesized using different metals and ligands as coordinating species were evaluated representing a wide diversity of surface areas, functionalities, structure

types, porosities and matrices. It was found that the Zr-based MOFs provide the highest gravimetric (726 F/g) and aerial (5.09 mF/cm^2) capacitance. **Figure 14a** shows the assembly of MOF-based symmetric supercapacitor. The explored MOFs show much better energy density as compared to activated carbon and graphene based electrode materials as shown in **Figure 14b**. **Table 2** summarizes the various MOFs used in this study with their cyclic stability.

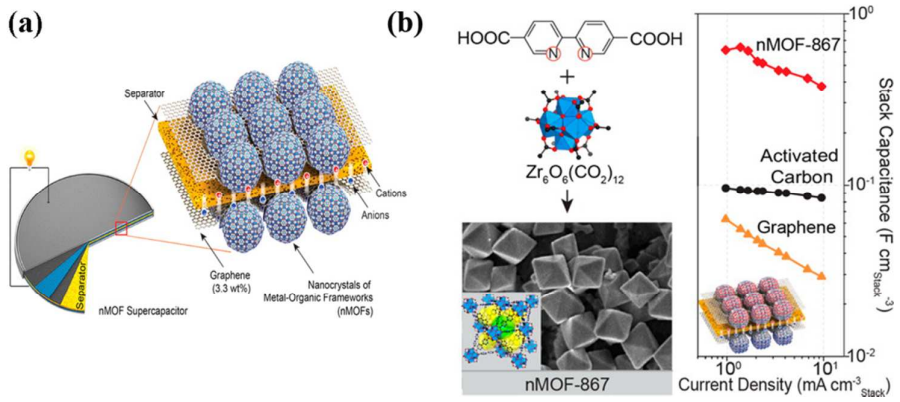

Figure 14. (a) Construct for nMOF supercapacitors. (b) Highest nMOF supercapacitor (nMOF-867) and comparison to activated carbon and graphene.[138] Reproduced with permission of American Chemical Society.

Table 2. Summary of the maximum stack and areal capacitance and life cycle for all nMOFs and related supercapacitors.[134]

nMOF/material	Max stack capacitance (F cm$_{stack}^{-3}$)	Max areal capacitance (mF cm$_{areal}^{-2}$)	life cycle[d]
nMOF-5	0.043	0.341	3500
nMTV-MOF-5-AB	0.029	0.232	10000

nMTV-MOF-5-AC	0.060	0.478	1600
nMTV-MOF-5-AD	0.072	0.566	>10000
nMTV-MOF-5-AE	0.122	0.913	3000
nMTV-MOF-5-AF	0.025	0.195	>10000
nMTV-MOF-5-ABC	0.100	0.790	3500
nMTV-MOF-5-ABCD	0.113	0.891	>10000
nMTV-MOF-5-ABCDE	0.095	0.752	2500
nMTV-MOF-5-ABCDEF	0.063	0.501	1500
nNi-MOF-74	0.052	0.415	4000
nCo-MOF-74	0.050	0.392	>10000
nM3M-MOF-74	0.056	0.443	4000
nM5M-MOF-74	0.106	0.834	800
nM7M-MOF-74	0.146	1.155	300
nHKUST-1	0.296	2.334	6000
nHKUST-1-NG[a]	0.041	0.324	
Cu-BTC-NPNC[b]	0.028	0.221	
nMOF-177	0.090	0.713	4000
nZIF-8	0.034	0.268	2500
nMOF-801	0.280	2.329	1400
nMOF-801-L[c]	0.036	0.284	1500

nUiO-66	0.246	1.945	7000
nUiO-67	0.093	0.736	>10000
nMOF-867	0.644	5.085	>10000
nMOF-808	0.068	0.540	5000
activated carbon	0.100	0.788	>10000
graphene	0.065	0.515	>10000

[a]NG, no graphene. [b]NPNC, no porosity and no crystallinity. [c]L, large-size nanocrystals. [d]The life cycle was determined by the number of cycles carried out until the capacitance dropped to 80% of the initial value.

Since several nanostructures can be derived from MOFs as explained in earlier sections, we will explore each of these nanostructures separately for supercapacitor applications. MOFs have been widely used to produce high surface area carbonaceous nanostructures. Controlling carbonaceous structures has attracted increased attention due to the good stability. In essence, the nanoporosity and accessible surface of the carbons are the most critical factors which determine their electrochemical performance. Carbon materials have shown very high surface areas with tailorable porosity which makes them very attractive candidates for electrochemical energy storage.[139,140] We demonstrated successful derivation of carbon from MOF templates for the first time and their application as supercapacitor electrodes.[77] MOF/glycerol composite derived carbon exhibited high surface area (2587 m^2/g) and excellent

electrochemical performance as electrode for supercapacitors (344 F/g @ 50 mA/g), proving the suitability of MOF derived carbon for supercapacitor applications.[78] Although first reports suggested the usage of MOF composites (MOF/glycerol, MOF/resorcinol-formaldehyde, MOF/furfuryl alcohol)[78,83,141,142] to derive carbon, further investigations led to derivation of carbon solely from pure MOF with improved electrochemical performances.[70] Recently, introduction of heterogeneous species (e.g. nitrogen) in the carbon structures has also triggered the improvements in the capacitive storage of carbonaceous materials. MOFs could provide inherent presence of nitrogen atoms in the ligands which would be retained in the resultant product upon carbonization, thus providing N-doped carbons. Nitrogen-rich ligand was used to synthesize IRMOF-3 like structure. Carbonization of these MOFs at 950 °C led to formation of N-rich carbonaceous species.[143] Such N-doped carbon with 3D structure exhibited high capacitance of 239 F/g at a scan rate of 5 mV/s (**Figure 15**). Very recently; derivation of N-doped carbons from ZIF-67 was also reported, demonstrating high amount of graphitic carbon could improve overall conductivity and capacitance.[144] The authors found the relative ratios of G bands to D bands (I_G/I_D) to be about 2.07 which is much higher (two times higher) than that of traditional activated carbon. The carbon consisted of narrow pore size distribution with majority of pores in the range of 2-5 nm and a pore volume of 0.84 cm^3/g. It exhibited a high capacitance value (238 F/g @ 20 mV/s) compared to other MOF derived carbon products. **Table 3** summarizes the different types of carbons from MOFs with their respective surface areas and capacitance performances.

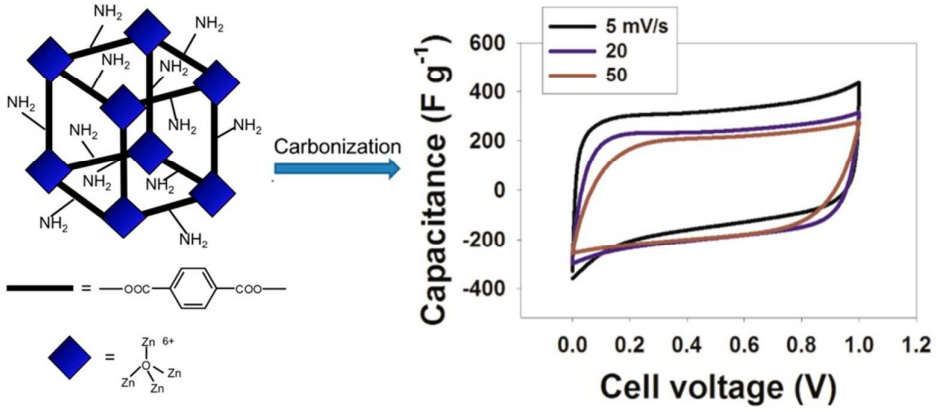

Figure 15. Supercapacitor application of nitrogen-containing MOF (IRMOF-3) derived carbon product.[143] Reproduced with permission of American Chemical Society.

Table 3. Surface area and capacitances of carbon derived from different MOF materials

Precursor	T[a](°C)	S[b](m^2/g)	V[c] (cm^3/g)	C[d] (F/g)	Ref.
MOF-5	1000	2872	2.06	204 @ 5mV/s	74
MOF-5	950	2587	3.14	344 @ 50 mA/g	75
MOF-5	500	2222	1.14	271 @ 2mV/s	80
MOF-5	600	1521	1.48	100 @ 5mV/s	137
ZIF-8	900	1215	0.57	214 @ 5mV/s	67
MOF-2	1000	1378	——	165 @ 10 mV/s	62
ZIF-69	1000	2264	2.16	168 @ 5 mV/s	79
ZIF-8	800	2972	2.56	211 @ 10 mV/s	68
IRMOF-3	950	553	0.34	239 @ 5 mV/s	139
ZIF-7	950	783	0.56	185 @ 25 mV/s	141
ZIF-67	800	943	0.84	238 @ 20 mV/s	140
Al-PCP	800	1103	1.04	174 @ 1 A/g	142

HKUST-1	800	50	1.46	83 @ 1 A/g	[142]

[a]T: carbonization temperature; [b]S: Brunauer–Emmett–Teller (BET) specific surface area; [c]V: pore volume; [d]C: specific capacitance.

A simple calcination in air was employed to convert Co-based MOF to obtain Co_3O_4 nanostructures for capacitive energy storage.[147] The resultant nanostructures exhibited specific capacitance of 208 F/g at current density of 1 A/g. High surface area Co_3O_4 nanostructures were further derived from Co-MOF with relatively smaller pore size distribution, exhibiting capacitance as high as 150 F/g at a discharge rate of 1 A/g.[31] Despite particularly high specific capacitances, MOs lack practical applications due to some fundamental issues such as low electrode surface area, poor conductivity and very short cycle life. The conductivity of the MO based electrodes drops drastically at higher charge/discharge rates owing to poor electron conduction in bulk and thus results in overall increase in resistance. This results in localized contribution from exposed electrode material close to current collector and little contribution from bulk material. Moreover, pure MOs are crystalline materials and the electrolyte can only diffuse to limited distances (~20 nm) inside the pores of crystalline materials as compared to amorphous materials where electrolyte can diffuse larger distances (~50 nm).[2] Based on these ideas, it is very important to develop electrode materials with high conductivity where upon MOs possess high surface areas and are of amorphous state in nature. Recently, layered double hydroxide nanocages based on Ni-Co from ZIF-67 were developed to obtain very

high capacitance (1203 F/g at current density of 1 A/g), which could partly address the inherent conductivity and exposed surface issues.[148] Another promising approach exploited widely is to fabricate the nanostructures on highly conductive substrate. MOFs are promising candidates in this regard owing to 3D porous networks and presence of metallic species in the frameworks, which can provide charge storage *via* both electrochemical double layer formation and a reversible redox reaction.[20,136] It has been suggested by several studies that carbon acts as an excellent substrate to decorate ultra-small MO particles.[149,150] Very recently, researchers demonstrated successful derivation of carbon matrix decorated with Fe_2O_3 by using PVP coated PB as template materials along with RF-PEO-PPO (resorcinol formaldehyde, polyethylene oxide and polypropylene oxide) triblock copolymer as extra carbon source.[151] The obtained composite consisted of small Fe_2O_3 nanoparticles (<50 nm) and had relatively higher surface area of 344 m^2/g (**Figure 16)**. It showed a high capacitance performance of 209 F/g at the scan rate of 0.2 A/g. MO/C composites have been very attractive in recent times for supercapacitor applications with performances above 1000 F/g due to presence of enhanced redox active species.

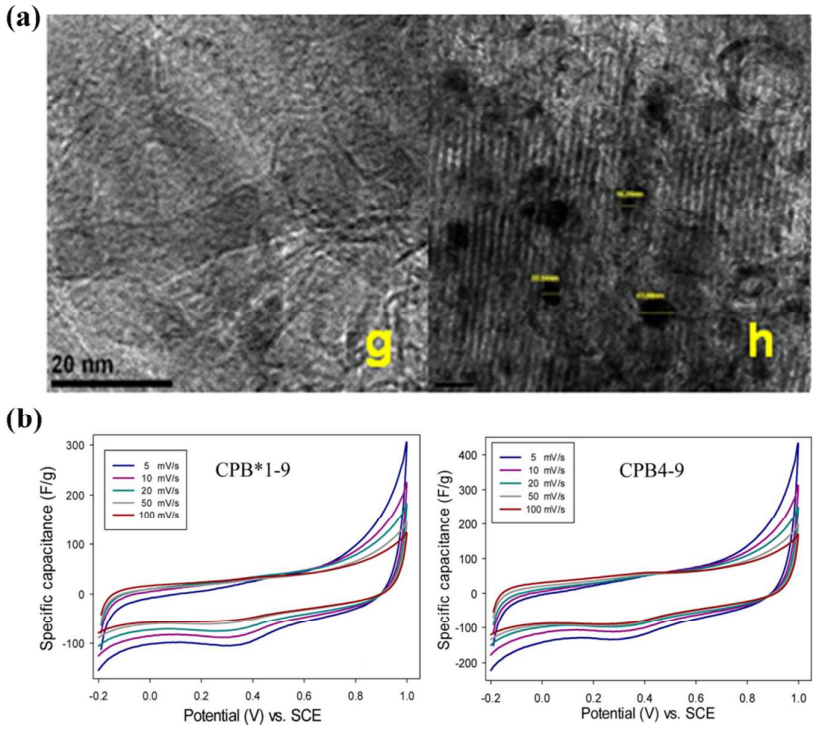

Figure 16. (a) High-resolution transmission electron microscopy (HRTEM) images for CPB*1−9 (g) and CPB4−9 (h). (b) Cyclic voltammetry (CV) curves for CPB*1−9 (A) and CPB4−9 (B) electrodes at various scan rates ranging from 5 mV s^{-1} to 100 mV.[151] Reproduced with permission of American Chemical Society.

Until now, very limited numbers of reports on derivation of MO/C composite from MOF have been reported for supercapacitor application, which greatly hinders the advancement in this field. Major problems arise due to following reasons:

i. At lower carbonization temperature, MOF decompose to give MO/C composite, but the carbon component has low graphitization degree and is highly resistive, which limits the performance.

ii. Higher carbonization temperature could lead to highly conductive carbon but MO is reduced M which is inactive for capacitive behavior.

So, it can be concluded that despite recent progress in MOFs for supercapacitor applications, there still remains a number of challenges which need further research efforts.

4.2 Batteries

Commercial market for portable devices has exponentially increased in its value in past couple of decades due to wide applications from mobiles to laptops. LIBs constitute a major unit of these portable devices as a charge house. Introduced in commercial market in 1990s, LIBs have progressed ever since at very fast rate due to certain fundamental advantages such as high energy density, long lifespan, environment friendly and no memory effect.[152-154] The basic principle for LIBs is that Li in anode materials is oxidized to Li^+ and move to the cathode where it is inserted into the cathode material. Despite considerable fast progress, development and application of these batteries were affected by some fundamental problems (such as electrode pulverization and low capacities). Primitive LIBs used graphite and $LiCoO_2$ as anode and cathode material, respectively. However, in modern times, their practical application is seriously hindered due to low theoretical capacity (372 mAh/g for graphite and 148 mAh/g for $LiCoO_2$). These LIBs anode based on graphite stored charges by insertion mechanism where Li^+ ions were reversibly inserted into the layered graphite structures. However, the cycle life of these batteries was compromised due to permanent blockage of insertion sites leading to decline in the performance. These primitive electrode materials were replaced with Li-alloys that

improved the capacities considerably, but accompanied by large volume changes which caused damages to the electrode and ultimately affected the performance. MOFs represent a highly porous framework which can accommodate these changes along with Li^+ storage sites and have been envisioned as a potential material for the battery electrodes. Since batteries consist of anode and cathode separated by a porous separator, it is very important to develop and modernize both of these electrodes.

4.2.1 Anodes Materials

The most common material used as anode is graphite, but its application is limited by low the capacity. Since MOFs have been exploited in pristine form as well as used to derive different materials as explained in previous section, here we will look into the MOF materials one after the other for LIB anodes. Pristine MOFs can be a replacement for the anode materials as they provide very large surface area and nanopores where Li^+ ions can undergo insertion during charging process. However, previous study showed that pristine MOFs were not suitable for reversible insertion of Li^+ ions in MOF because of the limited cycling capacity.[23] Zn-based MOF-177 was considered to undergo following reactions (1-3) with Li^+ ions during charging/discharging process where the reaction would lead to decomposition of the framework making it literally unsuitable for reversible reaction. The first reaction led to decomposition of the MOF structure while the third reaction is considered to be reversible which is responsible for the remaining capacity of the electrode material.

$$Zn_4O(BTB)_2(DEF)_m(H_2O)_n + e^- + Li^+ \rightarrow Zn + Li_2O \qquad (1)$$

$$DEF + H_2O + e^- + Li^+ \rightarrow Li_2(DEF) + LiOH \quad (2)$$

$$Zn + Li^+ + e^- \leftrightarrow LiZn \quad (3)$$

Despite early setbacks, researchers made a big progress in 2010 by using formate MOFs, $Zn_3(HCOO)_6$, $Co_3(HCOO)_6$ and $Zn_{1.5}Co_{1.5}(HCOO)_6$.[155] The introduction of the formate bridged MOFs kinetically favor the formation of lithium formate instead of the Li_2O that caused structure deterioration in the case of MOF-177. Lithium storage in these formate bridged MOFs proceed via the conversion reaction. For example, $Zn_3(HCOO)_6$, the best performed anode material in this report, reacted with Li to form Zn nanoparticles and lithium formate during the first discharge process (**Eq. (4)**), which followed by the formation of Li-Zn alloy after deep discharge to 0.005 V (**Eq. (5)**). In the charge process, the alloy turns back to Zn nanoparticles and zinc formate via the reverse process in discharge.

$$Zn_3(HCOO)_6 + 6Li^+ + 6e^- \leftrightarrow 3Zn + 6HCOOLi \quad (4)$$

$$3Zn + 3Li^+ + 3e^- \leftrightarrow 3LiZn \quad (5)$$

As a result, the formate bridged MOFs showed much improved Li-storage ability. $Zn_3(HCOO)_6$ displayed the best performance with a reversible capacity of 560 mAh/g after 60 cycles at the rate of 60 mA/g within the voltage window of 0.005-3.0 V (**Figure 17**). Though there is still some space between the scientific study and commercial utilization of MOFs as anode material, this work supports that MOFs can

be stabilized during charge/discharge process by judicious selection of ligand and metal center, and improved capacity and cycle performance can thus be expected.

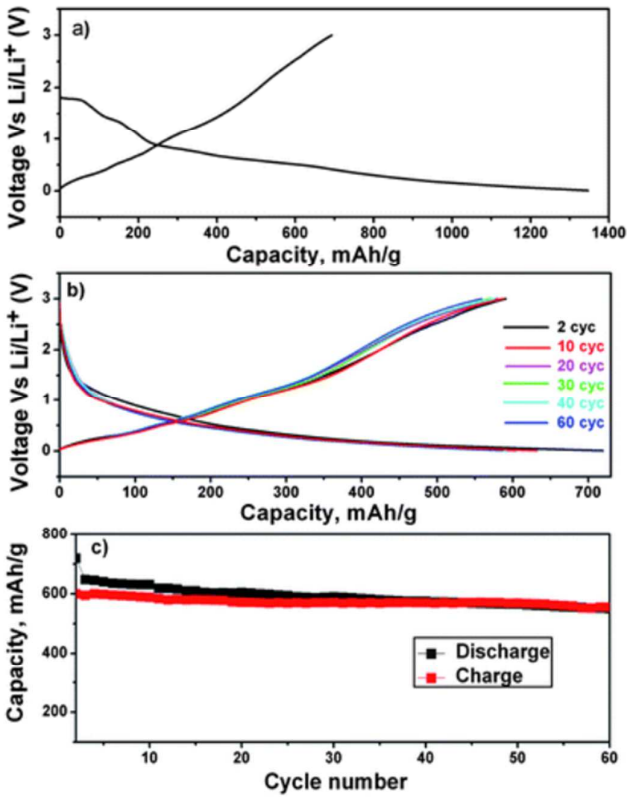

Figure 17. Charge-discharge profiles for $Zn_3(HCOO)_6$ anode (a) first cycle, (b) selected cycles and (c) cycling performance at the rate of 60 mA/g (0.11C).[155] Reproduced with permission of Royal Society of Chemistry.

Apart from using pristine MOFs for electrochemical applications, MOF derived materials are also getting wider attention as LIB anode materials. Given the fact that application of bulk metallic structures is limited by poor cyclic stability, metallic nanostructures are widely explored due to potentially large capacities under a high utilization degree. MOFs, owing to their high surface area and nanoporosity, provide ideal sacrificial templates to obtain nanoporous MOs or metal sulfide (MS)

with high surface area for LIBs.[156-162] Successful derivation of MOs from MOF was demonstrated for first time by us.[92] Co-MOF was heated in air at 600 °C to obtain agglomerated Co_3O_4 structures which delivered a capacity of >700 mAh/g at the discharge rate of 50 mA/g after 100 cycles, demonstrating considerably higher stability of MOs from MOFs. It is widely believed that hollow MO nanostructures could provide higher capacity and better stability. Kirkendall effect was explored to obtain porous Co_3O_4 nanocages from Prussian Blue analogue, $Co_3[Co(CN)_6]_2$, by calcination at 400 °C (**Figure 18a)**.[156] Heating at higher temperature led to decomposition of framework where MOF chains decomposed to form CO_2 and NO_x which then forced the metals to move to the outer directions leading to formation of unique morphologies such as porous shells with high surface areas. The resultant porous structure exhibited excellent capacitance of 1500 mAh/g at 300 mA/g and good rate capability with a capacity of 1090 mAh/g at 1500 mA/g, 974 mAh/g at 3000 mA/g, 720 mAh/g at 6000 mA/g, 535 mAh/g at 9000 mA/g and recover to 951 mAh/g at 1500 mA/g (**Figure 18b**). The superior battery performance was attributed to the textured nanostructure: i) the porous structure in walls is convenient for the diffusion Li^+ ions; ii) the high surface area of the hollow structure shortens the Li^+ diffusion length and reduces electrolyte resistance; iii) the decreased particle size increases the exposed atoms and the structural stain; iv) the coated amorphous carbon layer could accommodate the strain induced by volume change during cycling.

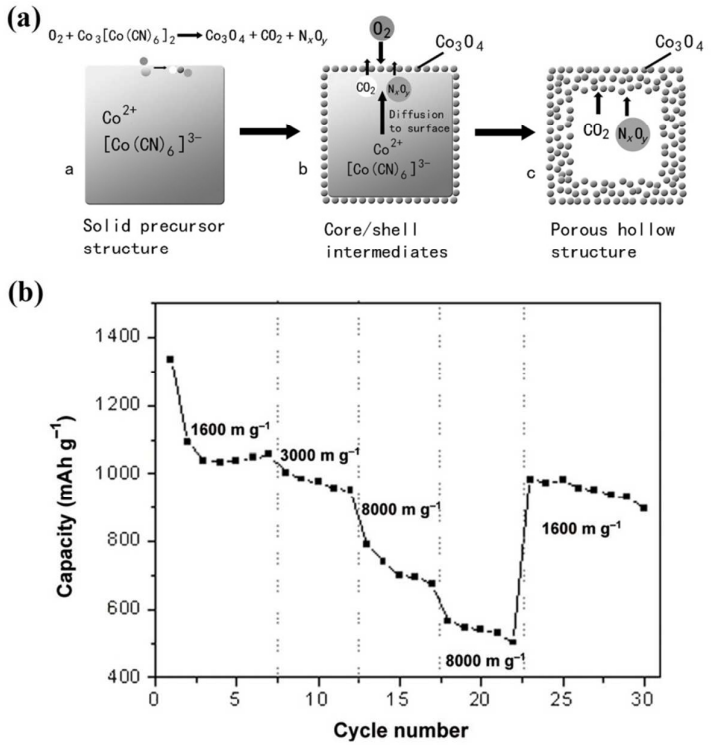

Figure 18. (a) Schematic of the procedure used to fabricate porous Co_3O_4 nanocages using $Co_3[Co(CN)_6]_2 \cdot nH_2O$ nanocubes are used as solid precursors. (b) Rate capability of the as-prepared Co_3O_4 porous nanocages.[156] Reproduced with permission of Wiley-VCH Verlag GmbH & Co. KGaA.

Several recent works reported the use of multi metallic oxides (such as spinel oxides) for LIBs with improved characteristics.[68,98,99,157] Researchers reported Fe_2O_3@$NiCo_2O_4$ hollow cubes derived from MOFs with multi metals as coordinating agents.[100] Authors proposed the following reactions during charging/discharging process. The composite showed a high capacity of 1080 mAh/g even after 100 cycles.

$$NiCo_2O_4 + 8Li^+ + 8e^- \rightarrow Ni + 2Co + 4Li_2O \quad (6)$$

$$Ni + Li_2O \rightarrow 4NiO + 2Li^+ + 2e^- \quad (7)$$

$$2Co + 2Li_2O_4 \rightarrow 2CoO + 4Li^+ + 4e^- \quad (8)$$

$$2CoO + 2/3Li_2O_4 \rightarrow 2/3Co_3O_4 + 4/3Li^+ + 4/3e^- \quad (9)$$

$$Fe_2O_3 + 6Li^+ + 6e^- \rightarrow 2Fe + 3Li_2O \quad (10)$$

These MOF-derived highly porous MOs can provide high capacities but their practical application is limited due to lack of long cycle life. In spite of relatively better stability as compared to pure MOs synthesized by traditional methods, the cyclic stability is still not good enough for these to be considered as potential candidates in commercial market. One possible solution to fully exploit metallic structures is to use carbon coated metallic species at nano scale[163-165] or decorate them on a highly conducting substrate.[166-168] Carbon coating on the metallic species is important to prevent agglomeration of the particles during charge/discharge process and to enhance the electrical conductivity of the composite. A Zn-based MOF, IRMOF-1 was used for derivation of high surface area carbon decorated with ZnO quantum dots (3.5 nm).[102] The authors suggested that the carbonization temperature and duration play critical role in defining the characteristic of the product. Carbonization of IRMOF-1 at 550 °C lead to the formation of carbon coated ZnO quantum dots without agglomeration. The synthesized product exhibit high capacity of ~1200 mAh/g at 75 mA/g and excellent charge storage reversibility (~100% capacity retention after 50 cycles). Similarly, MOF composites with highly conducting substrates lead to further improvement in the performance of the electrode materials by decorating MO on porous carbon or graphene. For instance, Fe-MOF composites with reduced graphene oxide (rGO) was synthesized, followed by

annealing to obtain highly porous composites of Fe_2O_3/3DGN (3DGN= three-dimensional graphene network).[169] **Figure 19** shows the schematic of synthesis as well as electrochemical behavior of the composites. The composite provided a high capacity of 864 mAh/g at 200 mA/g even after 50 cycles. Similarly, a composite material using ZIF-8 and chitosan was synthesized to obtain ZnO decorated carbon material.[170] The composite provided high capacity of 750 mAh/g at 50 mA/g.

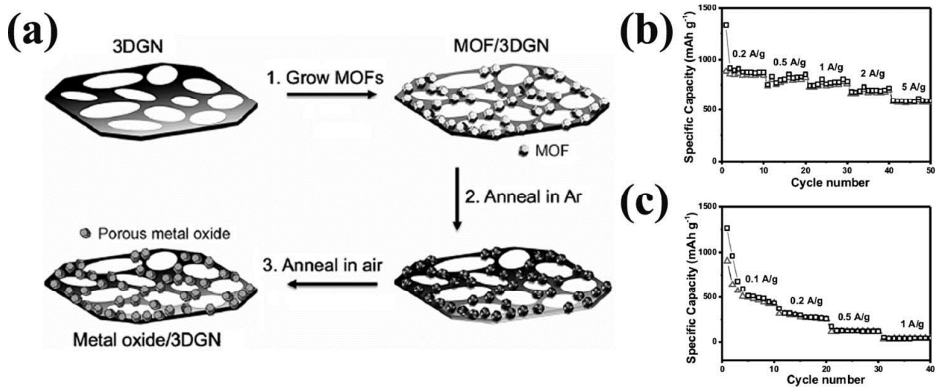

Figure 19. (a) Schematic illustration of the process used for the synthesis of metal oxide/3DGN composites. b,c) Rate capacity of electrodes composed of the Fe_2O_3/3DGN composite (b) and Fe_2O_3 (c). Square and triangle symbols indicate the discharge and charge specific capacities, respectively.[169] Reproduced with permission of Wiley-VCH Verlag GmbH & Co. KGaA.

4.2.2 Cathode Materials

Since the pioneering work have proved the suitability of MOFs for electrochemical applications especially as cathode materials in batteries,[24] the idea of mixed valence state was employed to obtain more stable M-O bonds in the MOF framework. Several transition metal (Fe^{III}, Cr^{III}, V^{III}) carboxylate based MOFs (more commonly known as MIL (*Materials of Institut Lavoisier*)) were explored in order to understand the reversible Li^+ ion storage process. Using several characterization tools, transition of

these metals in different oxidation states during charging and discharging processes was proved, which was found as the key in reversible Li^+ ion storage without MOF decomposition. Although these MOFs showed relatively lower capacities, this work was an interesting and important study as it opened an undisputed avenue towards charge storage in pristine MOFs. Subsequent studies further provided insights into reversible insertion of Li^+ ions in MOFs proving successful use of MOF as cathode for LIBs.[25-27] *In situ* X-ray absorption fine structure analysis (XAFS) was used to predict the Li^+ insertion in the MOF framework.[25] MIL-53 (Fe^{III} (OH, F)bdc; bdc=benzene-1,4 dicarboxylate) was selected to understand the insertion process. In continuation to Férey's work,[24] it was demonstrated that Li^+ insertion leads to reduction of Fe^{III} to Fe^{II} along with localized change in Fe-O and Fe-Fe bond lengths which are compensated by a small distortion in the long MOF chains during charge/discharge process. The insertion of Li^+ was further explained by density functional theory (DFT) simulations[26] and mixed valence structures[27] to provide insights into lithiation/delithiation process. The authors explored the redox mechanism of Fe in MIL-53 by varying Li^+ composition from xLi/Fe=0-1 and studying the most probable Li^+ sites using DFT, and they proved that lithiation/delithiation is completely reversible affecting the oxidation state of metals (**Figure 20a**). Using the DFT method, four possible insertion sites were identified as shown in **Figure 20b**. In essence, pristine MOFs have been successfully applied as cathode materials in LIBs which is still under consideration to address issues such as low capacity and capacity retention.

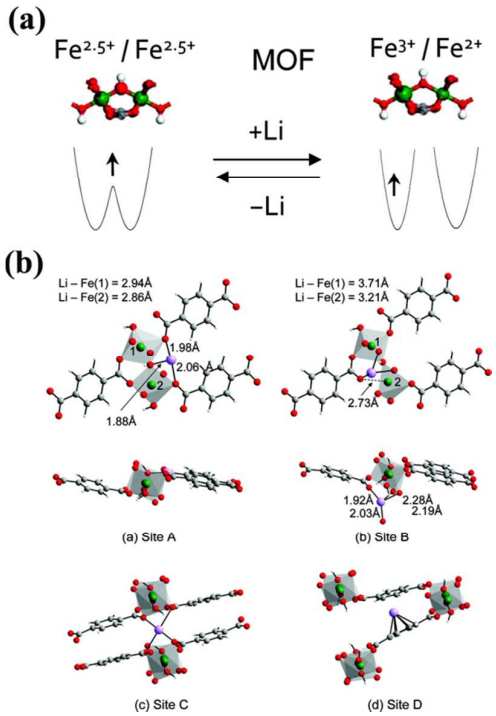

Figure 20. (a) Mixed valence state of the MOF upon reversible insertion of Li. (b) Results of the full structural relaxations performed at xLi/Fe = 0.25 for the MIL53(Fe)-F_0 system using the PW91 functional and U_{eff} = 5 eV for lithium sites (a) A, (b) B, (c) C, and (d) D.[26] Reproduced with permission of American Chemical Society.

Developing Na-ion battery as an alternative to Li-ion battery is raising more and more attentions due to the increasing demand on limited lithium sources. Despite the similarities in Na-ion batteries and Li-ion batteries, Na^+ ion is larger than the Li^+ ion, which requires a more open framework to reach a sufficient mobility of Na^+ ion in the cathode material. Possessing the highly open structure, some MOFs were thus explored as a candidate, especially the Prussian Blue ($A[Fe^{III}Fe^{II}(CN)_6]$, A = Na^+ or K^+) and its analogues ($K[MFe(CN)_6]$, M = Fe, Co, Ni, Cu, Zn).[21,171-173] As shown in **Figure 21a**, Prussian Blue has a cubic structure, and Fe^{III} and Fe^{II} alternatively locate on the corners of octahedra connected by $C{\equiv}N^-$. The Fe^{III} ions are coordinated to the

nitrogen ends of $C\equiv N^-$ groups while the Fe^{II} ions bond with their carbon ends. The C≡N bond opens the faces of sub-cubes forming a large ionic channel along the <100> direction. Moreover, only half of the body-center "A sites" in the structure are occupied, which enables Na^+ insertion/extraction.[173,174] The nitrogen-coordinated Fe^{III} was replaced with Cu^{II}, which produced copper hexacyanoferrate (CuHCF) nanoparticles with the Prussian Blue open framework structure in a low-cost and scalable method.[175] The electrodes showed long cycle life and high rate capability. However, the usage of aqueous electrolyte limits the stable voltage to only 1.5 V. The non-aqueous electrolyte system was also investigated with a series of Prussian Blue analogues. A high reversible plateau at 3.82 V and 3.56 V was found in the case of $KMn^{II}Fe^{III}(CN)_6$.[174] Later, researchers reported the removal of Na^+ ion in the analogues to obtain a 3.4 V cathode in half-cell.[176] They found that the sodium-ion concentration strongly affects product composition and structure. A phase transition from cubic to rhombohedral symmetry was found due to the Na^+ displacement along the [111] direction at high Na^+ concentration (**Figure 21b**). This transition is reversible by cycling the Na^+ concentration. As a result, the initially rhombohedral $Na_{1.72}MnFe(CN)_6$ exhibited a capacity of 134 mAh/g and retained 120 mAh/g after 30 cycles, which made it a promising cathode material for Na-ion batteries.

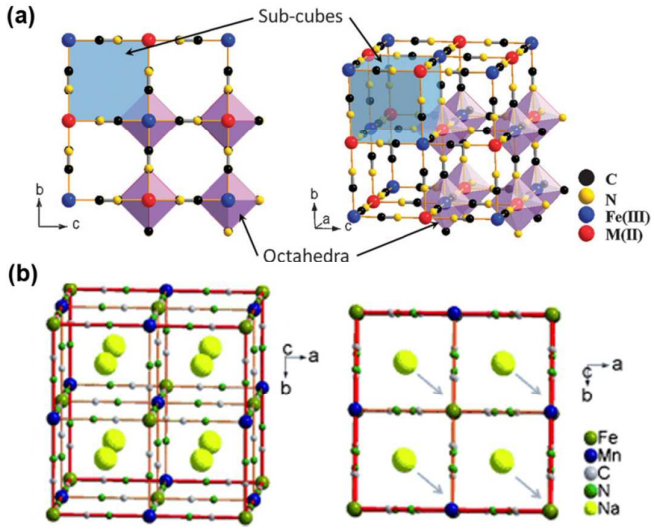

Figure 21. (a) Crystal structure of Prussian Blue analogues.[174] Reproduced with permission of Royal Society of Chemistry. (b) Crystal structure of a cubic sodium manganese hexacyanoferrate (left) and the alkali-ion displacement along [111] axis resulting in rhombohedreal symmetry (right).[176] Reproduced with permission of Wiley-VCH Verlag GmbH & Co. KGaA.

In addition to the MOFs that directly participate in redox reaction as cathode material, stable MOF with rich surface chemical environment and high porosity were also used as host to fabricate cathode composite with sulfur. Sulfur is a promising cathode material in lithium batteries.[177] Calculated from the sulfur redox reaction, it gives a high specific capacity of 1675 mAh/g and the corresponding energy density of the Li-S cell can reach 2600 Wh/kg. The value is 3 to 5 times higher than that of traditional lithium ion cell. However, sulfur suffers from low coefficient of utilization in bulk state and poor reversibility due the loss of active material during cycling.[178] To deal this problems, researchers have proprosed to disperse and confine sulfur at nanoscale by using nanoporous materials.[179-183] MOFs, with the tunable pore texture and rich surface chemical environment, could be a fancy host for sulfur. Pioneering work was led by using a mesoporous MOF named MIL-100(Cr) as host for sulfur

impregnation (**Figure 22**).[184] MIL-100(Cr) has a very-high surface area of nearly 3100 m^2/g and a fancy hierarchical pore structure with micropores of ~5-9 Å wide and mesopores of ~25-30 Å.[185] Sulfur was loaded into the pores of the MOF by a melt-diffusion strategy. Electrode prepared from the MOF/S composite displayed marked increase in capacity retention, which can be attribued to the nano confinement effect from the MOF cage that enable reversible capture and release of soluble polysulfides during the cycling. Besides MIL-101(Cr), other porous MOF hosts like HKUST-1,[186] ZIF-8,[187] Ni-MOF[188] and MIL-53(Al)[189] were also studied. From those results, we could summarize that the suitable pore structure (large pore and small windows) in MOFs enables the high loading of sulfur and the strong confinement to polysulfides.

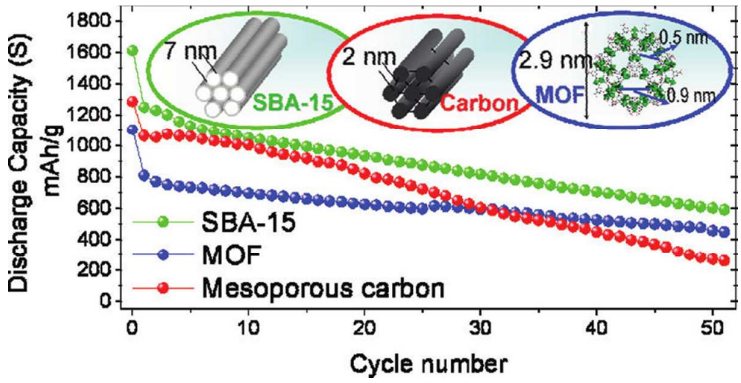

Figure 22. Comparison of the cycle performances of Li-S cells prepared from various host: SBA-15, MOF and mesoporous carbon.[184] Reproduced with permission of American Chemical Society.

Besides the enhanced confined environment from the porous structure, MOFs possess the rich surface activity that also exerts pronounced effect on the interactions between sulfur species and the MOF framework during the electrochemical process.

For example, MIL-100(Cr) has the oxygenated framework that brings about the O-S surface interaction in MIL-100(Cr)/S composite, helping to improve the cycle performance.[184] However, the functional groups in the framework may not always make the positive contribution. MIL-53(Al) and NH_2-MIL-53(Al) were compared as host for Li-S batteries and a worse performance was found in the latter one.[189] The amino groups in NH_2-MIL-53(Al) increase the energy barrier for charge transfer and also hinder the ion diffusion in the MOF channels. Moreover, an interaction between sulfur and open metal sites in MOFs was also suggested. HKUST-1/S composite were studied and the structure was revealed by both single and powder X-ray diffraction.[186] The crystal structure was established, which indicates the sulfur confinement due to pore spaces and open Cu^{2+} sites. The Cu(II)-S interactions in the composite were further demonstrated from X-ray photoelectron spectroscopy (XPS). The S_{2p} peaks shifted to lower energies due to the interactions. The existence of interactions between metal node and sulfur species has also been reported.[188] Those Lewis acid-base interactions between the open metal site and polysulfides showed great potential in improving the cycling performance of the MOF/S composite, which opens new avenues for the selection of MOF in this application. Considering the diverse functional groups (like -CH3, -OH, -NH2, *etc*.) in the organic framework and numerous choices of metal node, systematic researches on the interactions between MOF functional surface and polysulfides could be anticipated, which may be helpful for the rational design of sulfur host.

However, despite the good confinement effect, those MOFs are electronically insulating hosts, which leads to low sulfur utilization and poor rate performance in Li-S cells. Coupling MOF/S with advanced electron conducive carbon materials, such as graphene[190] and carbon nanotube,[191] appear to show improved electrochemical performance. In addition, the electron conductivity of the MOF host can be remarkably enhanced after high temperature activation. The organic frameworks in MOFs are converted to conductive carbons and the pores in the parent MOFs retain in the derived materials, which could make them good candidates as conducing matrix as well as hosts for sulfur.[81,192-195] In previous part, we introduced the three-dimensional carbon from Al-BTC aerogel. The hierarchical pore structure was found to be effective to construct C/S cathode. The macropores in this product could work as reservoirs for electrolyte and the mesopores act as transport paths while sulfur is confined by the micro- and mesopores. Due to the possible interaction enhancement effect from heteroatoms dopants, MOF-derived porous carbons with modified surface could be anticipated in improving the battery cycling performance.

4.3 Fuel Cells

Polymer electrolyte membrane fuel cells (PEMFCs) represent one of the most promising energy conversion systems associated with high energy density, attractive conversion efficiency and low environmental impact.[196,197] They breathe in fuel (hydrogen, methanol, ethanol or formic acid) and generate electricity via gentle electrochemical reactions. For example, in hydrogen fuel cells, hydrogen oxidation

reaction (HOR) takes place at the anode and gives off electrons that travel from the external circuit to the cathode and participate in oxygen reduction reaction (ORR) (**Figure 23**).[198] MOFs, which have been demonstrated to be indispensable for clean energy storage and conversion, have also shown great potential in fuel cells. MOFs possess numerous advantages such as the high surface area, rich functionalities and tunable pore structure to be used as electrocatalysts in electrodes as well as in fuel (H_2) generation and the electrolyte materials over the conventional materials for fuel cell application.[50] The great designability in MOFs enables the multi-roles in fuel cell application and throws lights on the principle of developing advanced fuel cell materials. The detailed advantages will be discussed in the following separate parts.

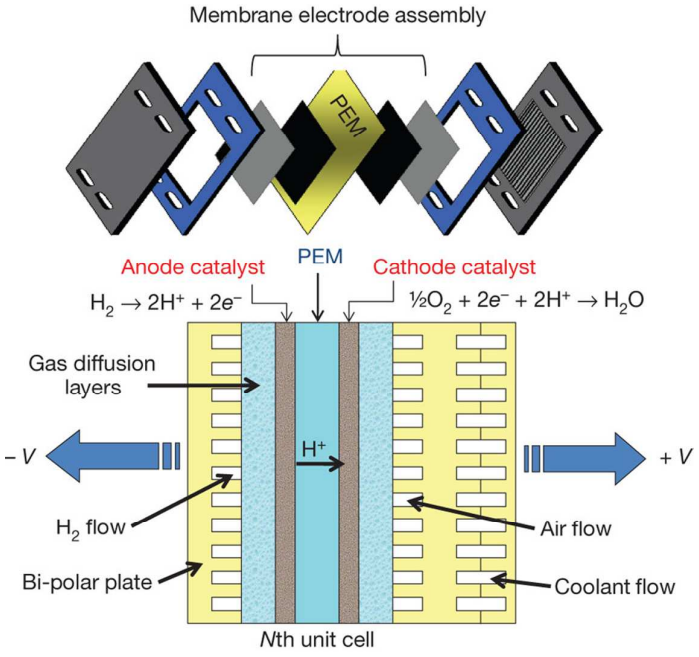

Figure 23. Fuel-Cell components.[198] Reproduced with permission of Nature Publishing Group.

4.3.1 Oxygen Reduction Reaction Catalysts

Considering that the PEMFCs operate at low temperatures (~80 °C), the two reactions in **Figure 23** must be speeded up with the help of efficient catalysts in order to achieve the desired high power density. The state-of-the-art catalysts are platinum and platinum alloys.[199,200] However, the high price and scarcity of platinum hinder the large scale application.[201] It is highly desirable to find efficient and inexpensive alternatives to platinum based catalysts for fuel cell reactions especially for the oxygen reduction reaction at cathode which requires much more platinum because of the slower reaction speed.[202] One of the major advances is the development of metal-nitrogen-carbon (M-N-C) catalysts from transition-metal macrocycle precursors. The early work found that cobalt phthalocyanine (CoPc) was active for ORR catalysis.[203] In order to obtain more stable catalysts, researchers applied the high temperature activation method to treat the macrocycle precursors.[204] Later, researchers substituted the macrocycles by mixtures of much cheaper transition-metal salts and nitrogen precursors, and they also obtained improved ORR activity and enhanced stability.[202,205,206] Though there are debates on the nature of the ORR active sites in these catalysts, the viewpoint that the ORR catalysts can be generated from the nitrogen and transition-metal rich precursors is commonly accepted. Besides the element composition, the microstructure of a catalyst also determines the performance. It has been suggested that the micropores in the catalyst are required for the catalytic activity.[205,207]

For these considerations, MOFs are the ideal candidate for preparing M-N-C catalysts. MOF precursors with rich M-N-C sites and tunable microstructure can be

achieved from precise molecular design. Although MOFs with transition-metal centers like Cu,[208-210] Fe[211] and Co[212] have shown some ORR catalytic activity, the performance of pure MOFs was limited due to their low electron conductivities and poor stabilities. It was since the first example of MOF derived ORR catalyst by activating a cobalt imidazolate frameworks (CoIM) at high temperature that more attention has been paid to this field.[213] In CoIM, each cobalt atom is four coordinated by nitrogen atoms from the imidazolate ligand (**Figure 24a**). There are abundant Co-N_4 moieties within the MOF. It was estimated that in a single crystal of CoIM, the number of Co-N_4 sites could reach as high as 3.6×10^{21} cm^{-3}, which could be utilized to generate the catalytic center with a high density in the pyrolyzed samples. Though the long-range ordered structure in the parent MOF was destroyed after thermal activation, a high surface area and a significant fraction of the micropore retained. All of them, put together, contributed to the high catalytic activity toward oxygen reduction with an onset potential of 0.83 V and half-wave potential of 0.68 V in acidic medium (**Figure 24b**). Note that the onset potential of Co-based ORR catalysts is typically 0.1 V less than that of Fe-based catalysts,[213,214] the cobalt center was substituted by iron, resulting in the iron imidazolate (FeIM) framework (**Figure 24c**).[215] FeIM derived catalyst displayed better activity than that of CoIM, and the performance was further improved by improved by mixing with a Zn^{II} zeoliticimidazolate framework, ZIF-8. The best performed catalyst showed a high onset potential of 0.915 V and a half-wave potential of 0.755 V (**Figure 24d**). The

corresponding singe cell test of this catalyst demonstrated a current density of 12 A/cm^3 at 0.8 V.

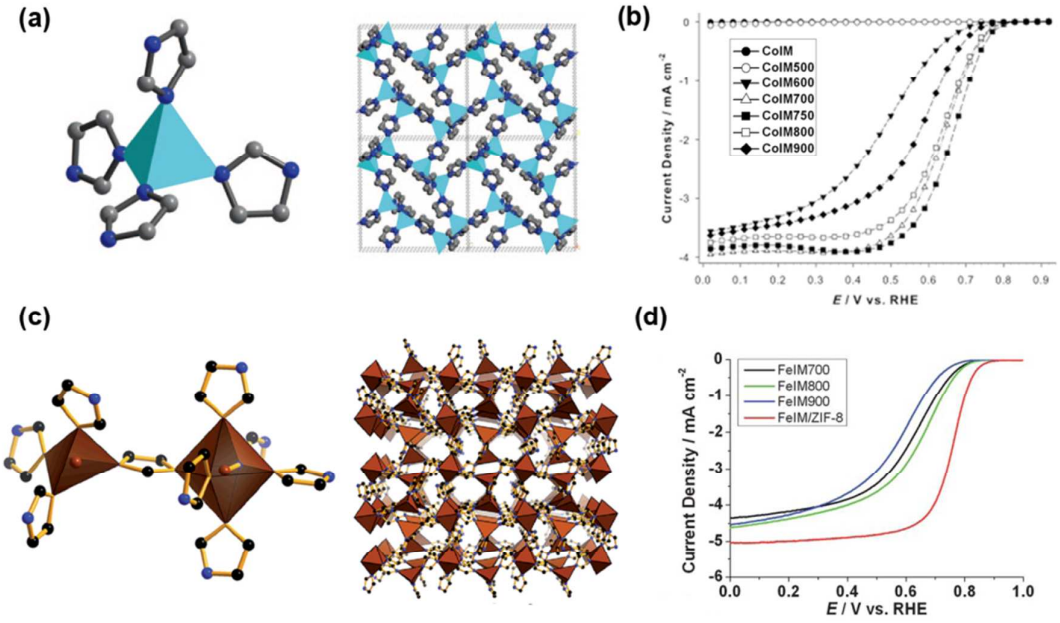

Figure 24. (a) Coordination geometries in CoIM frameworks (grey, C; blue, N; turquoise, Co). (b) ORR polarization curves for CoIM samples treated at different temperatures.[213] Reproduced with permission of Wiley-VCH Verlag GmbH & Co. KGaA. (c) Coordination geometries in FeIM frameworks (black, C; blue, N; brown, Co). (d) ORR polarization curves for FeIM samples treated at different temperatures.[215] Reproduced with permission of Royal Society of Chemistry.

ZIF-8 is a typical subclass of MOF material with a high surface area of nearly 1800 m^2/g. It has already been commercialized (Basolite Z1200, BASF). The use of ZIF-8 is designed to provide a microporous host in catalyst system considering that the micropores benefit the catalytic activity. Moreover, the rich nitrogen sites in ZIF-8 itself can be converted to nitrogen doped in carbon that is active for ORR.[30,216] ZIF-8 was introduced as alternative to conventional carbon supports in ORR catalyst.[217] ZIF-8 was loaded with phenanthroline and ferrous acetate. After simple heat treatment,

they obtained quite good electrocatalyst that can deliver a volumetric activity of 230 A/cm^3 at $0.8V_{iR\text{-}free}$, which is among the best performances for non-precious metal catalysts. Based on an improved understanding in the coordination chemistry of this system, the synthesis of ZIF-8 based catalyst precursor was optimized by milling $FeAc_2$, 2,4,6-tris(2-pyridyl)-*s*-triazine (TPTZ) with ZIF-8.[218] They found that iron nuclei on the surface of ZIF-8 particles were advantageous as compared to dispersion inside the ZIF-8 because the derived catalytic similar FeN_x sites were more accessible to ORR-related species, like oxygen and protons. This finding demonstrates the importance of structure design in ORR catalyst.

Oxygen reduction occurs at the triple-phase boundary among oxygen, electrolyte and catalyst. To ensure an efficient transport of oxygen, protons and electrolyte in ORR catalysts, their structures need to be carefully designed. We first brought this idea to attention by finding that reduction in the size of MOF precursors can significantly improve the catalytic activity of their derived ORR catalysts.[219] Through precise control on the growth condition for ZIF-67, a series of ZIF-67 crystal with the size from micrometers to nanometers were obtained (**Figure 25**). By reducing the particle size of the catalyst, more catalytic surface was expected to be exposed, which was verified by our observation. The smallest mono-dispersed ZIF-67 nanocrystal derived catalyst delivered rather good ORR performance in acidic solution with an onset potential of 0.86 V and half-wave potential of 0.71 V. The kinetic current density was also significantly higher than that of the larger samples, suggesting that the higher surface-to-volume ratio can benefit a better catalysis

performance. This good improvement from the downsizing of MOF materials for ORR application opens new avenues for the designing of MOFs and their flourishing application, especially in electrochemical energy storage and conversion.

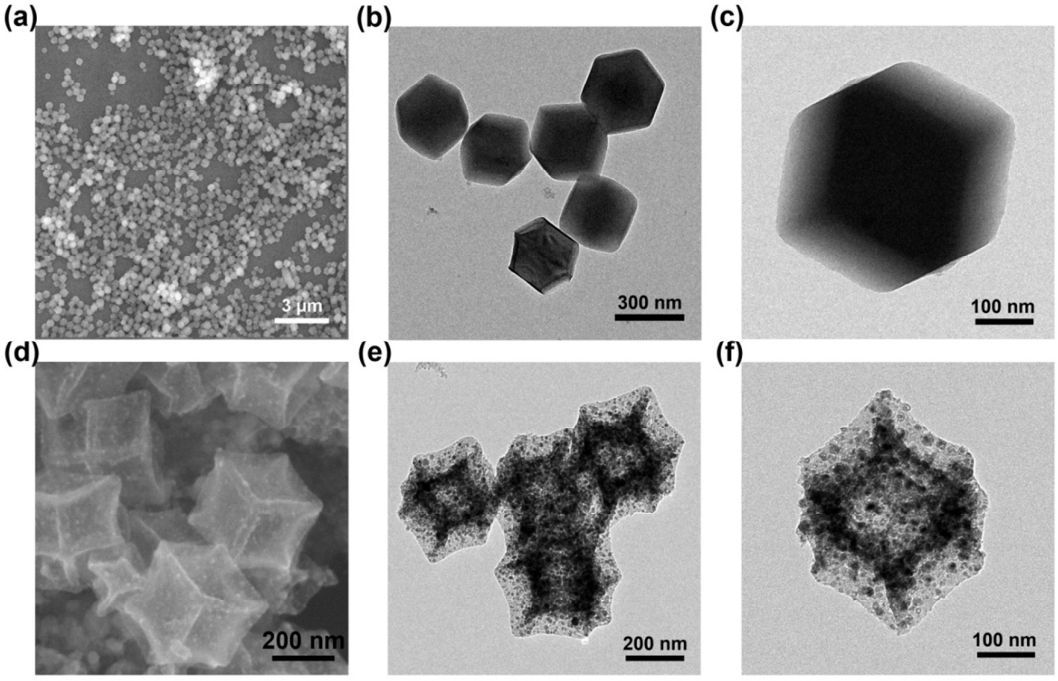

Figure 25. SEM (a) and TEM (b,c) images of ZIF-67 nanocrystal. SEM (c) and TEM (c,d) images of the derived catalyst.[219]

MOFs, as described in the previous parts, could be tailored with high surface area and regular porous structure that are beneficial for fabricating good ORR catalysts. However, these advantages might not exist in the pyrolyzed samples in which the ordered pores have been destroyed at high temperatures. These pores in MOF-derived catalysts are mainly disordered and non-interconnected, still not efficient for mass transport inside the samples. A deep thinking on how to obtain MOF-derived three-dimensionally ordered pore structures is highly desirable in

further improving the electrochemical performance. Recently, we introduced a general route to fabricate MOF-derived catalyst with the ideal open structure for ORR catalysis.[75] A cobalt-benzimidazole MOF was introduced into the confined space of an extra hard template, CMK-3, which is an ordered porous carbon matrix. The cobalt ions from MOF were used as metal source to generate Co metal cores and the nitrogen-rich organic ligands were turned into nitrogen-doped carbon shell on the Co cores after heat treatment. They were later transformed into fancy Co@Co_3O_4@C nanoparticles embedded in CMK-3 via a controlled oxidation procedure. The obtained product has three-dimensional interconnected ordered pores which provides better diffusion pathway for oxygen and electrolyte than the disordered single MOF-derived structure (**Figure 26**). As a result, it shows an ORR onset potential as high as 0.93 V and half-wave potential of 0.81 V, which ranks it among the best performed non-precious metal catalysts. The performance is almost identical to the commercial Pt/C and the current density is even higher in the potential range of 0.6-0.8 V. Modifying MOF structure for advanced ORR catalysts attracts increasing attention.[90,220] Recently, a Te nanowire-directed templating method was reported to synthesize ZIF-8 nanofibers with high aspect ratio and tunable diameters.[221] After subsequent heat treatment, the ZIF-8 nanofibers were transformed into nitrogen doped carbon with hierarchical pores and complex network. This fancy structure also contributes to the very high electrocatalytic activity for ORR.

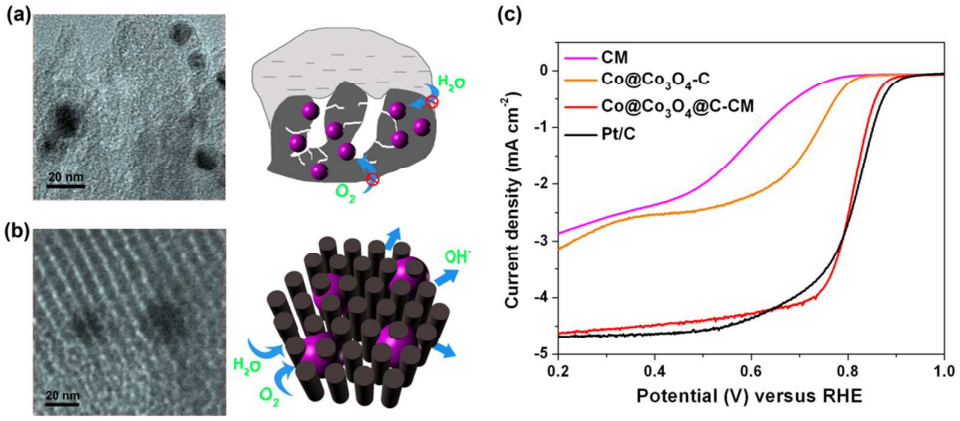

Figure 26. Schematic illustration of structures of the catalysts from pure MOF (a) and MOF-CM composite. (c) ORR polarization curves of the CM, $Co@Co_3O_4$-C (from pure MOF), $Co@Co_3O_4$@C-CM (from MOF-CM composite) and Pt/C.[75]

The strategy of fabricating advanced ORR catalysts from MOFs can be concluded as two routes: element selection and structure modification. Although the nature of active center in MOF derived M-N-C catalysts is not clear, nitrogen in these system contribute to the catalytic activity by donating electrons to carbon. Due to the diversity of the ligands we can use to fabricate MOF precursors, other heteroatoms (such as sulfur, phosphorus) doped catalysts could be obtained and expected to show distinct properties. Moreover, from precise control over the MOF structure or combination with other template, advanced ORR catalyst with superior mass transport properties could be anticipated.

4.3.2 Hydrogen/Oxygen Evolution Reaction Catalysts

Hydrogen and oxygen are a prerequisite for generating power from the PEMFCs. Though there are several sources from which researchers can obtain hydrogen and oxygen to feed PEMFCs, electro-driven transforming water into hydrogen or/and

oxygen stands out due to its relative gentle condition and environmentally friendly character. This transformation involves two half reactions: hydrogen evolution reaction (HER, $2H^+ + 2e^- \rightarrow H_2$) and oxygen evolution reaction (OER, $2h^+ + H_2O \rightarrow 1/2O_2 + 2H^+$), which can be viewed as reverse reactions of hydrogen oxidation and oxygen reduction described in the previous parts.[222,223] Hydrogen/oxygen can be produced when applying excess potential over the thermodynamic potential for HER/OER. However, operations at the large overpotential from this way could be a waste of energy. This problem can be moderated by using catalysts which remarkably reduces the overpotential.[224] It is highly desirable, but is of great challenge to develop advanced catalysts for the two reactions. In recent years, researchers have managed to generate hydrogen or oxygen from water by utilizing MOF-based electrochemical catalysts.

Some MOFs with transition-metal nodes have been demonstrated as HER or/and OER active.[225-229] It was found that a copper-centered MOF on graphene oxide (GO) had catalytic activities toward both HER and OER.[209] The Cu-MOF is constructed from copper nitrate trihydrate, 1,4-benzenedicarboxylic acid (bdc) and triethylene-diamine (ted). As shown in **Figure 27a**, the Cu-MOF possesses $Cu_2(COO)_4(ted)_2$ secondary building units, which are linked by bdc to form the two-dimensional network. These networks are further connected by ted leading to the final three-dimensional framework. GO sheets are rich in OH and epoxy groups on both sides, so the addition of GO sheets can contribute to an integral component of MOF framework by linking the MOF nodes, which further affected MOF

crystallization and electrochemical performance. **Figure 27b** showed the HER performance of Cu-MOF with different amount of GO addition. Cu-MOF (GO: 8 wt%) sample had very promising HER activity with an onset potential of -0.087 V (reversible hydrogen electrode, RHE), which is close to that of Pt/C (0.013 V). The current density at -0.4 V reached as high as 122.5 mA/cm^2 although it is lower than Pt/C (313 mA/cm^2). The target material also exhibited very good OER activity (**Figure 27c**). In the Cu-MOF/GO composite, copper is catalytically active. The surrounding nitrogen and oxygen atoms, with the electron-accepting abilities, polarize the copper nodes in the framework. Moreover, the addition of high surface area GO enhanced the electron transfer in the composite, further improving the catalytic activity.

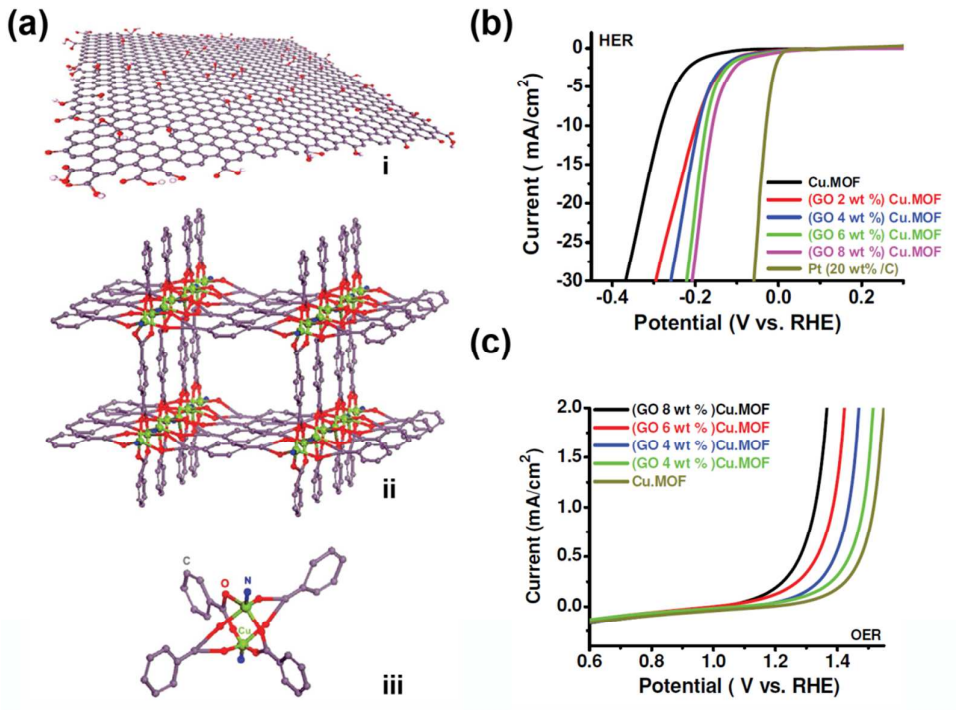

Figure 27. (a) Chemical structure of GO (i) and coordination geometries in Cu-MOF (ii, iii). (b) Hydrogen evolution reaction and (c) oxygen evolution reaction activities of various catalysts.[209] Reproduced with permission of Wiley-VCH Verlag GmbH & Co. KGaA.

In most cases, HER or OER catalysts were produced in the form of particle agglomerates that were later transformed into thin film coated on electrodes like nickel foam or glassy carbon. However, the resulting catalyst layers do not possess the ideal structure for HER or OER which involves multiphase boundaries during the reaction. In an advanced electrocatalyst, the catalytic centers should have full contact with the electrolyte, and the generated H_2 or O_2 gas gets free outlets from the electrode. Recently, an advanced three-dimensional nanostructure by directly growing MOF nanowire arrays on Cu foil was reported (**Figure 28**).[230] The MOF precursor, Co-naphthalene dicarboxylate, was directly grown on a Cu foil from simple hydrothermal reaction at 80 °C. Then the MOF was converted into Co_3O_4/C composite after heat treatment in nitrogen atmosphere. The original nanowire morphology of parent MOF retained in the derived product, with the addition of extra micro- and meso-pores. Due to the strong binding between Co_3O_4/C nanowires and the Cu foil current collector, there were good electrical conductivity and high structural stability in the composite. The resultant material can thus be directly used as working electrode for OER without extra binders. OER performance test of the composite showed an excellent activity with an onset potential of ~1.47 V (RHE), which is very close to the IrO_2/C noble-metal catalyst (~1.45 V). Noticeably, it displayed much higher OER current density than IrO_2/C even at the same loading.

The resultant catalyst also possesses high stability. Even on a high voltage of 1.80 V, the Co_3O_4/C nanowires still had a close contact with the Cu foil.

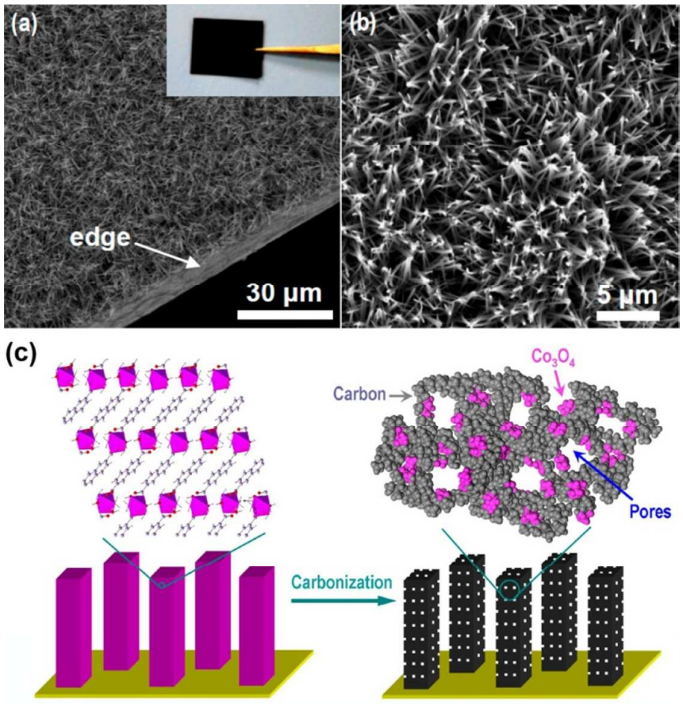

Figure 28. (a,b) SEM and (inset in a) optical image of Co_3O_4-C nanowire arrays. (c) Schematic illustration of Co_3O_4-C nanowire arrays formation on Cu foil.[230] Reproduced with permission of American Chemical Society.

4.3.3 Electrolytes

In fuel cells, proton conductor plays a crucial role since it determines the transport of the ionic species through the cell. Although proton conductors have been explored for a long time, the field is still lacking an efficient proton conductor material at academic as well as commercial level. Proton conduction in the electrolytes follows two basic mechanisms including Grotthuss (proton hopping) and vehicular (self-diffusion of proton species) mechanisms.[231-234] Despite recent progress, a major problem faced by proton conductor electrolytes is the design of materials in finding out whether

ordering and porosity is suitable for mobility or amorphous and dense structure are preferred. Most of the explored materials range from metal oxides to organic polymers, however they have conflicting properties in different papers and are not able to completely grasp the required properties.[44] The practical usage is further limited by temperature requirements for fuel cell operation, which change in a wide range from very low temperatures to highly elevated temperatures. Coordination polymers (CPs), also known as MOFs, have been studied for their conduction properties since 1979.[235,236] However, it was not until very recently that MOFs emerged as new and excellent replacements to traditional proton conduction materials at room temperature as well as at higher temperatures (>100 °C).[237-244] The possibility of using MOFs as proton conductors was demonstrated via using a Cu-based MOF to obtain a 2D structured compound that can conduct proton by the formation of H_3O^+ ions (conductivity ~1.5 $\times 10^{-5}$ S/cm).[245] The idea was further explored by using ferrous oxalate dihydrate which gave 1-D arrays of water molecules providing pathway for proton conduction (1.3 $\times 10^{-3}$ S/cm at 25 °C).[246] Although the proton conductivities were relative low, these initial works provided a new platform for the search of best material for solid electrolyte in fuel cells. Subsequent works explored bimetallic MOFs as solid electrolytes for proton conduction. Cr-MOF with various concentrations of Mn, Fe or Co was used[238] to generate 2D honeycomb layers, and tri(3-hydroxypropyl) ammonium was used to balance the charges on the framework. Researchers obtained a homogenous hydrophilic layer for proton conduction as shown in **Figure 29a**. Along with the conduction behavior, these MOFs also exhibited

another very interesting property of ferromagnetism which would affect the proton conduction capabilities.[247,248] Multi metal (Mn, Fe, Co) bridged together with organic ligands was developed to generate MOF with both ferromagnetism and proton conduction.[238,240] The resulting MOFs consisted of chains with hydroxyl networks which acted as mediator for transport of protons. A transition from paramagnetism to ferromagnetism was also observed, however, the effect on proton conduction and mechanism is still unclear.

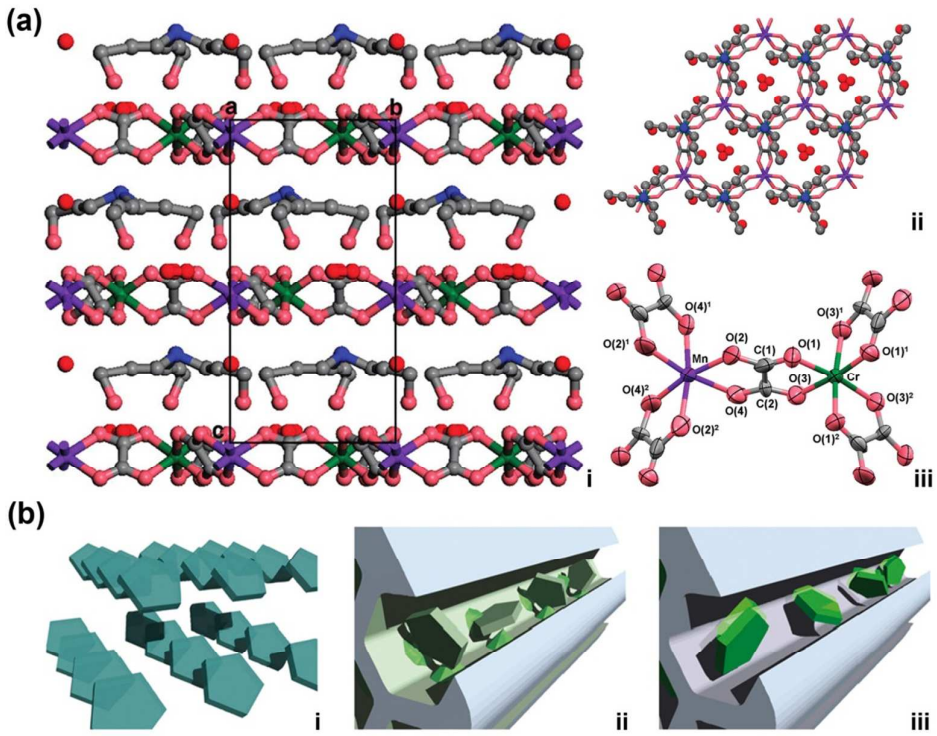

Figure 29. (a) Coordination geometries in $\{NH(prol)_3\}[MnCr(ox)_3]\cdot 2H_2O$. i) along the crystallographic *a* axis. ii) along the *b* axis. iii) scheme of the metal nodes (green, Cr; purple, Mn; red, oxygen).[238] Reproduced with permission of American Chemical Society. (b) Free and confined Imidazole molecules lead to different proton conductivities. i) Imidazole molecules are densely packed in the bulk solid. ii) Imidazole molecules are confined in a nanochannel. The wall of the channel contains active sites that have strong affinity to imidazole and reduce the mobility, which leads to the low proton conductivity. iii) Imidazole molecules in a nanochannel without strong binding to the wall show high mobility, resulting in the high proton conductivity.[249] Reproduced with permission of Nature Publishing Group.

The literature included above addressed proton conduction at low temperatures, which is dominated by the presence of hydroxyl species. However, conduction in anhydrous form at elevated temperatures is quite different. The use of host guest interactions to introduce proton conductivity at temperature above 100 °C was suggested.[249] It was proposed that encapsulation of proton conductor inside framework could effectively provide a plausible solution (**Figure 29b**). Imidazole was introduced into the nanochannels of as-synthesized MOF (as post synthesis modification), which produced composite materials with a high conductivity of 2.2×10^{-5} S/cm at 120 °C. A subsequent work reported a highly conductive MOF (5×10^{-4} S/cm at 150 °C in anhydrous H_2) with a similar host guest interactions.[250] Sodium trihydroxybenzene-trisulfonate was used to generate a 3D honeycomb structure with oxygen atoms available for conduction in the framework at elevated temperatures, exhibiting conductivity of 5.0×10^{-6} S/cm in hydrated form (different models of proton conductor shown in **Figure 30a**). However, dehydration principally led to reduction in conductivity (10^{-8} S/cm at 70 °C). 1*H*-1,2,4-triazole has also been reported to be potential proton conductor.[251] Previous study suggested that introducing 1*H*-1,2,4-triazole as guest molecules improved the conductivity of MOF at higher temperatures.[250] Although several reports suggested the use of MOFs in the hydrated or anhydrous forms, using single MOF in both forms has rarely been reported. Very recently, a Zn-based 3D MOF bridged the gap between the two exploited regions (low temperature and high temperature regions) of proton-conducting MOFs.[252] The MOF consists of an overall anionic framework built from Zn-oxalate units. This anionic

framework was interpenetrated by a supramolecular net $[(Me_2NH_2)_3(SO_4)]_n^+$ as shown in **Figure 30b**. The hydrated MOF exhibits highest conductivity reported to date for a MOF-based proton conductor (4.2×10^{-2} S/cm at 25 °C) maintaining a high conductivity of 1.0×10^{-4} S/cm under anhydrous condition (150 °C). Despite considerable progress, there is still a need to develop novel MOF materials which can overcome practical issues such as poor stability (in water, under stress, under differential temperatures) and relatively low conductivity. Application of MOFs in this field is still in growing phase and is considered to overcome the inherent issues and become one complete family of solid electrolytes.

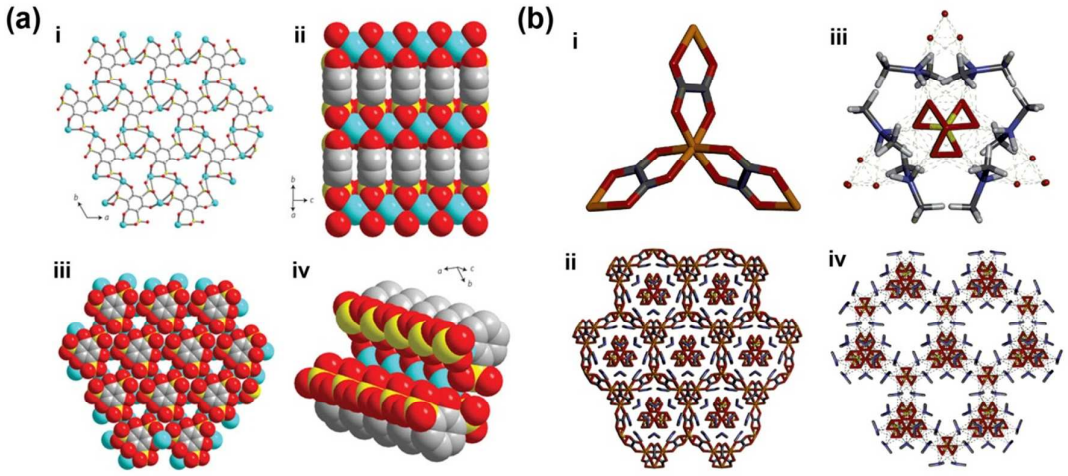

Figure 30. (a) Single-crystal X-ray structure of β-PCMOF2. Grey, C; red, O; yellow, S; cyan, Na. i) A ball-and-stick representation of a single layer showing the open 18-membered channels. ii) A space-filling diagram perpendicular to the pores, showing the packing of the aryl groups down the crystallographic c-axis. iii) A space-filling diagram down the axis of the pores. iv) A space-filling diagram of the cross-section of one pore, showing the high degree of sulfonation.[250] Reproduced with permission of Nature Publishing Group. (b) i) The tris-chelated D_3-symmetric $[Zn_2(ox)_3]^{2-}$ subunit. ii) Crystal structure of $\{[(Me_2NH_2)_3(SO_4)]_2[Zn_2(ox)_3]\}_n$. iii) Hydrogen bonding interactions between dimethyl ammonium cations and sulfate anions. iv) 3D supramolecular $[(Me_2NH_2)_3SO_4]^+_n$ net formed by hydrogen bonding between dimethyl ammonium cations and sulfate anions. C gray, N blue, O red, S yellow, Zn orange.[252] Reproduced with permission of Wiley-VCH Verlag GmbH & Co. KGaA.

5. Summary and Prospective

Search for novel materials with wider applications has been the purpose of recent researches. Until now, no single material has exhibited a wider range of applications in comparison to MOFs. MOFs have developed exponentially in the previous decade for various applications (from catalysis to sorption), but most recent researches are focused on developing nanoporous materials for energy storage and conversion. Utilizing the inherent properties of these highly ordered structures (surface area, pore size distribution, tenability using various functional groups, *etc*.) provide a unique feature which is not possible for other materials. Similarly, post treatment methods can also be used to tune the MOF structures for targeted applications. Other than using pristine MOFs, the possibility of synthesizing high surface area, ordered, meso- or microporous carbonaceous materials further enhance their possible applications.

In this review, we have summarized the recent progress from application-based designing of MOFs to the synthesis of various nanostructures using MOFs as template/sacrificial materials, especially for electrochemical properties. It is quite clear that MOFs can be designed both theoretically as well as experimentally. A researcher can generate a high surface area, ordered MOF with very small pore sizes using a singular metallic and ligand sources, while multi-metallic or multi-ligand approach can also be utilized to obtain application-oriented MOF structures. Using different ligands and metal centers, it is possible not only to tailor the MOF backbones but also to obtain various kinds of functional groups as well as open metal

sites for catalytic applications. The possibility to tailor MOFs, especially regarding the conduction properties, has been efficiently utilized in constructing functional materials for energy storage and conversion applications. Although earlier works suggested the unsuitability of MOFs in electrochemical applications, pioneering works have proved that pristine MOFs can be efficiently utilized for Li^+ ion insertion in LIBs. MOFs have also been successfully used for capacitive energy storage even in the as-synthesized form without any further modifications, which further elaborates their flexibility in electrochemical application.

Although pristine MOFs could be used for electrochemical energy storage, it is the derivation of several types of MOF-derived nanostructures that opened new avenues towards their successful usage. MOFs have been used as sacrificial templates to generate highly oriented nanostructures including carbon, metal oxides, metal carbide, metal sulfide and their composites. MOF-derived carbons and metal oxides have high surface areas and very narrow pore size distributions, showing high performances as electrode materials for supercapacitors and batteries. Similarly, presence of nanostructured redox active species on highly conductive substrate could be easily tailored using MOF templates, which adds more opportunities in designing efficient materials for enhanced energy storage. Despite the various pyrolyzed MOF nanostructures, a precise control on the fine structures of these materials is still absent because of the limited knowledge on the transformation process. For example, the surface area of MOFs would increase or decrease in the pyrolyzed forms. A deep understanding of this issue is of urgent need, which can be very helpful in designing

and constructing fine nanostructures from MOFs with high surface area, regular pores and tunable composition for electrochemical energy storage and conversion.

Acknowledgements

The authors are pleased to acknowledge the fine work of the talented and dedicated graduate students, postdoctoral fellows, and colleagues who have worked with us in this area and whose names can be found in the references. The authors would like to thank Peking University and AIST for financial support.

References

1. N. S. Choi, Z. Chen, S. A. Freunberger, X. Ji, Y. K. Sun, K. Amine, G. Yushin, L. F. Nazar, J. Cho and P. G. Bruce, *Angew. Chem. Int. Ed.*, 2012, **51**, 9994-10024.
2. Q. Lu, J. G. Chen and J. Q. Xiao, *Angew. Chem. Int. Ed.*, 2013, **52**, 1882-1889.
3. O. M. Yaghi and H. Li, *J. Am. Chem. Soc.*, 1995, **117**, 10401-10402.
4. H. Furukawa, K. E. Cordova, M. O'Keeffe and O. M. Yaghi, *Science*, 2013, **341**, 1230444.
5. H. Furukawa, N. Ko, Y. B. Go, N. Aratani, S. B. Choi, E. Choi, A. O. Yazaydin, R. Q. Snurr, M. O'Keeffe, J. Kim and O. M. Yaghi, *Science*, 2010, **329**, 424-428.
6. H. Deng, S. Grunder, K. E. Cordova, C. Valente, H. Furukawa, M. Hmadeh, F. Gandara, A. C. Whalley, Z. Liu, S. Asahina, H. Kazumori, M. O'Keeffe, O. Terasaki, J. F. Stoddart and O. M. Yaghi, *Science*, 2012, **336**, 1018-1023.
7. O. Shekhah, H. Wang, M. Paradinas, C. Ocal, B. Schupbach, A. Terfort, D. Zacher, R. A. Fischer and C. Woll, *Nat. Mater.*, 2009, **8**, 481-484.
8. P. Horcajada, T. Chalati, C. Serre, B. Gillet, C. Sebrie, T. Baati, J. F. Eubank, D. Heurtaux, P. Clayette, C. Kreuz, J.-S. Chang, Y. K. Hwang, V. Marsaud, P.-N. Bories, L. Cynober, S. Gil, G. Ferey, P. Couvreur and R. Gref, *Nat. Mater.*, 2010, **9**, 172-178.
9. K. M. L. Taylor-Pashow, J. D. Rocca, Z. Xie, S. Tran and W. Lin, *J. Am. Chem. Soc.*, 2009, **131**, 14261-14263.
10. M. E. Foster, J. D. Azoulay, B. M. Wong and M. D. Allendorf, *Chem. Sci.*, 2014, **5**, 2081-2090.
11. C. Y. Lee, O. K. Farha, B. J. Hong, A. A. Sarjeant, S. T. Nguyen and J. T. Hupp, *J. Am. Chem. Soc.*, 2011, **133**, 15858-15861.
12. J. M. Taylor, R. K. Mah, I. L. Moudrakovski, C. I. Ratcliffe, R. Vaidhyanathan and G. K. H. Shimizu, *J. Am. Chem. Soc.*, 2010, **132**, 14055-14057.
13. S. C. Sahoo, T. Kundu and R. Banerjee, *J. Am. Chem. Soc.*, 2011, **133**, 17950-17958.

14. R. Banerjee, H. Furukawa, D. Britt, C. Knobler, M. O'Keeffe and O. M. Yaghi, *J. Am. Chem. Soc.*, 2009, **131**, 3875-3877.
15. E. Jeong, W. R. Lee, D. W. Ryu, Y. Kim, W. J. Phang, E. K. Koh and C. S. Hong, *Chem. Commun.*, 2013, **49**, 2329-2331.
16. T. Rodenas, I. Luz, G. Prieto, B. Seoane, H. Miro, A. Corma, F. Kapteijn, F. X. L. i. Xamena and J. Gascon, *Nat. Mater.*, 2015, **14**, 48-55.
17. R. Q. Zou, H. Sakurai, S. Han, R. Q. Zhong and Q. Xu, *J. Am. Chem. Soc.*, 2007, **129**, 8402-8403.
18. R. Q. Zou, H. Sakurai and Q. Xu, *Angew. Chem. Int. Ed.*, 2006, **45**, 2542-2546.
19. M. A. Nasalevich, R. Becker, E. V. Ramos-Fernandez, S. Castellanos, S. L. Veber, M. V. Fedin, F. Kapteijn, J. N. H. Reek, J. I. van der Vlugt and J. Gascon, *Energy & Environmental Science*, 2015, **8**, 364-375.
20. R. Díaz, M. G. Orcajo, J. A. Botas, G. Calleja and J. Palma, *Mater. Lett.*, 2012, **68**, 126-128.
21. X. Wu, W. Deng, J. Qian, Y. Cao, X. Ai and H. Yang, *J. Mater. Chem. A*, 2013, **1**, 10130-10134.
22. L. Yang, S. Kinoshita, T. Yamada, S. Kanda, H. Kitagawa, M. Tokunaga, T. Ishimoto, T. Ogura, R. Nagumo, A. Miyamoto and M. Koyama, *Angew. Chem. Int. Ed.*, 2010, **49**, 5348-5351.
23. X. Li, F. Cheng, S. Zhang and J. Chen, *J. Power Sources*, 2006, **160**, 542-547.
24. G. Férey, F. Millange, M. Morcrette, C. Serre, M.-L. Doublet, J.-M. Grenèche and J.-M. Tarascon, *Angew. Chem. Int. Ed.*, 2007, **46**, 3259-3263.
25. G. d. Combarieu, S. Hamelet, F. Millange, M. Morcrette, J.-M. Tarascon, G. Férey and R. I. Walton, *Electrochem. Commun.*, 2009, **11**, 1881-1884.
26. C. Combelles, M. B. Yahia, L. Pedesseau and M. L. Doublet, *J. Phys. Chem. C*, 2010, **114**, 9518-9527.
27. C. Combelles, M. Ben Yahia, L. Pedesseau and M. L. Doublet, *J. Power Sources*, 2011, **196**, 3426-3432.
28. C. Wang, Z. Xie, K. E. deKrafft and W. Lin, *J. Am. Chem. Soc.*, 2011, **133**, 13445-13454.
29. J.-K. Sun and Q. Xu, *Energy Environ. Sci.*, 2014, **7**, 2071-2100.
30. A. Aijaz, N. Fujiwara and Q. Xu, *J. Am. Chem. Soc.*, 2014, **136**, 6790-6793.
31. F. Meng, Z. Fang, Z. Li, W. Xu, M. Wang, Y. Liu, J. Zhang, W. Wang, D. Zhao and X. Guo, *J. Mater. Chem. A*, 2013, **1**, 7235-7241.
32. J. D. Evans, C. J. Sumby and C. J. Doonan, *Chem. Soc. Rev.*, 2014, **43**, 5933-5951.
33. E. A. Flügel, A. Ranft, F. Haase and B. V. Lotsch, *J. Mater. Chem.*, 2012, **22**, 10119-10133.
34. Z. Zhang and M. J. Zaworotko, *Chem. Soc. Rev.*, 2014, **43**, 5444-5455.
35. S. Furukawa, J. Reboul, S. Diring, K. Sumida and S. Kitagawa, *Chem. Soc. Rev.*, 2014, **43**, 5700-5734.
36. S. Qiu and G. Zhu, *Coordination Chemistry Reviews*, 2009, **253**, 2891-2911.
37. D. Zacher, R. Schmid, C. Wöll and R. A. Fischer, *Angew. Chem. Int. Ed.*, 2011, **50**, 176-199.
38. S. T. Meek, J. A. Greathouse and M. D. Allendorf, *Adv. Mater.*, 2011, **23**, 249-267.

39. J. Gascon, A. Corma, F. Kapteijn and F. X. Llabrés i Xamena, *ACS Catal.*, 2014, **4**, 361-378.
40. A. Dhakshinamoorthy and H. Garcia, *Chem. Soc. Rev.*, 2014, **43**, 5750-5765.
41. Y. J. Colón and R. Q. Snurr, *Chem. Soc. Rev.*, 2014, **43**, 5735-5749.
42. M. D. Allendorf, C. A. Bauer, R. K. Bhakta and R. J. Houk, *Chem. Soc. Rev.*, 2009, **38**, 1330-1352.
43. Y. He, W. Zhou, G. Qian and B. Chen, *Chem. Soc. Rev.*, 2014, **43**, 5657-5678.
44. P. Ramaswamy, N. E. Wong and G. K. H. Shimizu, *Chem. Soc. Rev.*, 2014, **43**, 5913-5932.
45. M. Yoon, K. Suh, S. Natarajan and K. Kim, *Angew. Chem. Int. Ed.*, 2013, **52**, 2688-2700.
46. V. Stavila, A. A. Talin and M. D. Allendorf, *Chem. Soc. Rev.*, 2014, **43**, 5994-6010.
47. B. Van de Voorde, B. Bueken, J. Denayer and D. De Vos, *Chem. Soc. Rev.*, 2014, **43**, 5766-5788.
48. S.-L. Li and Q. Xu, *Energy Environ. Sci.*, 2013, **6**, 1656-1683.
49. A. Morozan and F. Jaouen, *Energy Environ. Sci.*, 2012, **5**, 9269-9290.
50. Y. Ren, G. H. Chia and Z. Gao, *Nano Today*, 2013, **8**, 577-597.
51. R. Q. Zou, L. Jiang, H. Senoh, N. Takeichi and Q. Xu, *Chem. Commun.*, 2005, 3526-3528.
52. O. Shekhah, H. Wang, D. Zacher, R. A. Fischer and C. Wöll, *Angew. Chem. Int. Ed.*, 2009, **48**, 5038-5041.
53. J. Cravillon, R. Nayuk, S. Springer, A. Feldhoff, K. Huber and M. Wiebcke, *Chem. Mater.*, 2011, **23**, 2130-2141.
54. K. Otsubo, Y. Wakabayashi, J. Ohara, S. Yamamoto, H. Matsuzaki, H. Okamoto, K. Nitta, T. Uruga and H. Kitagawa, *Nat. Mater.*, 2011, **10**, 291-295.
55. T. Fukushima, S. Horike, H. Kobayashi, M. Tsujimoto, S. Isoda, M. L. Foo, Y. Kubota, M. Takata and S. Kitagawa, *J. Am. Chem. Soc.*, 2012, **134**, 13341-13347.
56. Q. Gao, Y.-B. Xie, J.-R. Li, D.-Q. Yuan, A. A. Yakovenko, J.-H. Sun and H.-C. Zhou, *Cryst. Growth Des.*, 2012, **12**, 281-288.
57. T. Li, M. T. Kozlowski, E. A. Doud, M. N. Blakely and N. L. Rosi, *J. Am. Chem. Soc.*, 2013, **135**, 11688-11691.
58. M. Beidaghi and Y. Gogotsi, *Energy Environ. Sci.*, 2014, **7**, 867-884.
59. J. Zhang and X. S. Zhao, *ChemSusChem*, 2012, **5**, 818-841.
60. J. Chmiola, G. Yushin, Y. Gogotsi, C. Portet, P. Simon and P. L. Taberna, *Science*, 2006, **313**, 1760-1763.
61. J. Chmiola, C. Largeot, P. L. Taberna, P. Simon and Y. Gogotsi, *Angew. Chem. Int. Ed.*, 2008, **47**, 3392-3395.
62. Y. Ren, A. R. Armstrong, F. Jiao and P. G. Bruce, *J. Am. Chem. Soc.*, 2009, **132**, 996-1004.
63. D. Umeyama, S. Horike, M. Inukai, T. Itakura and S. Kitagawa, *J. Am. Chem. Soc.*, 2012, **134**, 12780-12785.
64. P. Pachfule, B. P. Biswal and R. Banerjee, *Chem. Eur. J.*, 2012, **18**, 11399-11408.
65. H. B. Aiyappa, P. Pachfule, R. Banerjee and S. Kurungot, *Cryst. Growth Des.*, 2013, **13**, 4195-4199.

66. Q. Lu, Z. J. Mellinger, W. Wang, W. Li, Y. Chen, J. G. Chen and J. Q. Xiao, *ChemSusChem*, 2010, **3**, 1367-1370.
67. Q. Lu, M. W. Lattanzi, Y. Chen, X. Kou, W. Li, X. Fan, K. M. Unruh, J. G. Chen and J. Q. Xiao, *Angew. Chem. Int. Ed.*, 2011, **50**, 6847-6850.
68. L. Zhang, H. B. Wu and X. W. Lou, *J. Am. Chem. Soc.*, 2013, **135**, 10664-10672.
69. Y. Sharma, N. Sharma, G. V. Subba Rao and B. V. R. Chowdari, *Adv. Funct. Mater.*, 2007, **17**, 2855-2861.
70. W. Chaikittisilp, M. Hu, H. Wang, H.-S. Huang, T. Fujita, K. C. W. Wu, L.-C. Chen, Y. Yamauchi and K. Ariga, *Chem. Commun.*, 2012, **48**, 7259-7261.
71. A. J. Amali, J.-K. Sun and Q. Xu, *Chem. Commun.*, 2014, **50**, 1519-1522.
72. A. Banerjee, K. K. Upadhyay, D. Puthusseri, V. Aravindan, S. Madhavi and S. Ogale, *Nanoscale*, 2014, **6**, 4387-4394.
73. M. Hu, J. Reboul, S. Furukawa, L. Radhakrishnan, Y. Zhang, P. Srinivasu, H. Iwai, H. Wang, Y. Nemoto, N. Suzuki, S. Kitagawa and Y. Yamauchi, *Chem. Commun.*, 2011, **47**, 8124-8126.
74. W. Cho, Y. H. Lee, H. J. Lee and M. Oh, *Chem. Commun.*, 2009, 4756-4758.
75. W. Xia, R. Q. Zou, L. An, D. G. Xia and S. J. Guo, *Energy Environ. Sci.*, 2015, **8**, 568-576.
76. H. R. Moon, D. W. Lim and M. P. Suh, *Chem. Soc. Rev.*, 2013, **42**, 1807-1824.
77. B. Liu, H. Shioyama, T. Akita and Q. Xu, *J. Am. Chem. Soc.*, 2008, **130**, 5390-5391.
78. D. Yuan, J. Chen, S. Tan, N. Xia and Y. Liu, *Electrochem. Commun.*, 2009, **11**, 1191-1194.
79. M. Hu, J. Reboul, S. Furukawa, N. L. Torad, Q. Ji, P. Srinivasu, K. Ariga, S. Kitagawa and Y. Yamauchi, *J. Am. Chem. Soc.*, 2012, **134**, 2864-2867.
80. H. L. Jiang, B. Liu, Y. Q. Lan, K. Kuratani, T. Akita, H. Shioyama, F. Zong and Q. Xu, *J. Am. Chem. Soc.*, 2011, **133**, 11854-11857.
81. W. Xia, B. Qiu, D. Xia and R. Zou, *Sci. Rep.*, 2013, **3**, 1935.
82. Q. Wang, W. Xia, W. Guo, L. An, D. Xia and R. Zou, *Chem. Asian J.*, 2013, **8**, 1879-1885.
83. J. Hu, H. Wang, Q. Gao and H. Guo, *Carbon*, 2010, **48**, 3599-3606.
84. S. Lim, K. Suh, Y. Kim, M. Yoon, H. Park, D. N. Dybtsev and K. Kim, *Chem. Commun.*, 2012, **48**, 7447-7449.
85. W. Chaikittisilp, K. Ariga and Y. Yamauchi, *J. Mater. Chem. A*, 2013, **1**, 14-19.
86. J. S. Li, S. L. Li, Y. J. Tang, K. Li, L. Zhou, N. Kong, Y. Q. Lan, J. C. Bao and Z. H. Dai, *Sci. Rep.*, 2014, **4**, 5130.
87. S. J. Yang, T. Kim, J. H. Im, Y. S. Kim, K. Lee, H. Jung and C. R. Park, *Chem. Mater.*, 2012, **24**, 464-470.
88. A. J. Amali, H. Hoshino, C. Wu, M. Ando and Q. Xu, *Chem. Eur. J.*, 2014, **20**, 8279-8282.
89. L. Chen, J. Bai, C. Wang, Y. Pan, M. Scheer and X. You, *Chem. Commun.*, 2008, 1581-1583.
90. P. Zhang, F. Sun, Z. Xiang, Z. Shen, J. Yun and D. Cao, *Energy Environ. Sci.*, 2014, **7**, 442-450.

91. R. Zboril, L. MaChala, M. Mashlan and V. Sharma, *Cryst. Growth Des.*, 2004, **4**, 1317-1325.
92. B. Liu, X. Zhang, H. Shioyama, T. Mukai, T. Sakai and Q. Xu, *J. Power Sources*, 2010, **195**, 857-861.
93. W. Cho, S. Park and M. Oh, *Chem. Commun.*, 2011, **47**, 4138-4140.
94. X. Xu, R. Cao, S. Jeong and J. Cho, *Nano Lett.*, 2012, **12**, 4988-4991.
95. Z. Wang, L. Zhou and X. W. David Lou, *Adv. Mater.*, 2012, **24**, 1903-1911.
96. L. Zhang, H. B. Wu, S. Madhavi, H. H. Hng and X. W. Lou, *J. Am. Chem. Soc.*, 2012, **134**, 17388-17391.
97. P. Mahata, D. Sarma, C. Madhu, A. Sundaresen and S. Natarajan, *Dalton Trans.*, 2011, **40**, 1952-1960.
98. J. Zhao, F. Wang, P. Su, M. Li, J. Chen, Q. Yang and C. Li, *J. Mater. Chem.*, 2012, **22**, 13328-13333.
99. L. Hu, Y. Huang, F. Zhang and Q. Chen, *Nanoscale*, 2013, **5**, 4186-4190.
100. G. Huang, L. Zhang, F. Zhang and L. Wang, *Nanoscale*, 2014, **6**, 5509-5515.
101. V. P. Santos, T. A. Wezendonk, J. J. Jaen, A. I. Dugulan, M. A. Nasalevich, H. U. Islam, A. Chojecki, S. Sartipi, X. Sun, A. A. Hakeem, A. C. Koeken, M. Ruitenbeek, T. Davidian, G. R. Meima, G. Sankar, F. Kapteijn, M. Makkee and J. Gascon, *Nat. Commun.*, 2015, **6**, 6451.
102. S. J. Yang, S. Nam, T. Kim, J. H. Im, H. Jung, J. H. Kang, S. Wi, B. Park and C. R. Park, *J. Am. Chem. Soc.*, 2013, **135**, 7394-7397.
103. R. Das, P. Pachfule, R. Banerjee and P. Poddar, *Nanoscale*, 2012, **4**, 591-599.
104. C. Wang, K. E. deKrafft and W. Lin, *J. Am. Chem. Soc.*, 2012, **134**, 7211-7214.
105. Y. Pan, B. Yuan, Y. Li and D. He, *Chem. Commun.*, 2010, **46**, 2280-2282.
106. F. Schröder, D. Esken, M. Cokoja, M. W. E. van den Berg, O. I. Lebedev, G. Van Tendeloo, B. Walaszek, G. Buntkowsky, H.-H. Limbach, B. Chaudret and R. A. Fischer, *J. Am. Chem. Soc.*, 2008, **130**, 6119-6130.
107. L. He, Y. Liu, J. Liu, Y. Xiong, J. Zheng, Y. Liu and Z. Tang, *Angew. Chem. Int. Ed.*, 2013, **52**, 3741-3745.
108. Y. Wei, S. Han, D. A. Walker, P. E. Fuller and B. A. Grzybowski, *Angew. Chem. Int. Ed.*, 2012, **51**, 7435-7439.
109. M. Müller, S. Hermes, K. Kähler, M. W. E. van den Berg, M. Muhler and R. A. Fischer, *Chem. Mater.*, 2008, **20**, 4576-4587.
110. Y. K. Park, S. B. Choi, H. J. Nam, D. Y. Jung, H. C. Ahn, K. Choi, H. Furukawa and J. Kim, *Chem. Commun.*, 2010, **46**, 3086-3088.
111. D.-W. Lim, J. W. Yoon, K. Y. Ryu and M. P. Suh, *Angew. Chem. Int. Ed.*, 2012, **51**, 9814-9817.
112. A. Aijaz, T. Akita, N. Tsumori and Q. Xu, *J. Am. Chem. Soc.*, 2013, **135**, 16356-16359.
113. F. Schröder, S. Henke, X. Zhang and R. A. Fischer, *Eur. J. Inorg. Chem.*, 2009, **2009**, 3131-3140.
114. N. Cao, L. Yang, H. Dai, T. Liu, J. Su, X. Wu, W. Luo and G. Cheng, *Inorg. Chem.*, 2014, **53**, 10122-10128.

115. M. S. El-Shall, V. Abdelsayed, A. E. R. S. Khder, H. M. A. Hassan, H. M. El-Kaderi and T. E. Reich, *J. Mater. Chem.*, 2009, **19**, 7625-7631.
116. X. Gu, Z.-H. Lu, H.-L. Jiang, T. Akita and Q. Xu, *J. Am. Chem. Soc.*, 2011, **133**, 11822-11825.
117. H.-L. Jiang, T. Akita, T. Ishida, M. Haruta and Q. Xu, *J. Am. Chem. Soc.*, 2011, **133**, 1304-1306.
118. J. Li, Q.-L. Zhu and Q. Xu, *Chem. Commun.*, 2014, **50**, 5899-5901.
119. Q. L. Zhu, J. Li and Q. Xu, *J. Am. Chem. Soc.*, 2013, **135**, 10210-10213.
120. J. Li, Q.-L. Zhu and Q. Xu, *Catal. Sci. Technol.*, 2015, **5**, 525-530.
121. M. Meilikhov, K. Yusenko, D. Esken, S. Turner, G. Van Tendeloo and R. A. Fischer, *Eur. J. Inorg. Chem.*, 2010, **2010**, 3701-3714.
122. L. Ma, C. Abney and W. Lin, *Chem. Soc. Rev.*, 2009, **38**, 1248-1256.
123. A. Dhakshinamoorthy and H. Garcia, *Chem. Soc. Rev.*, 2012, **41**, 5262-5284.
124. J. Juan-Alcañiz, J. Gascon and F. Kapteijn, *J. Mater. Chem.*, 2012, **22**, 10102-10118.
125. M. Yoon, R. Srirambalaji and K. Kim, *Chem. Rev.*, 2012, **112**, 1196-1231.
126. A. Aijaz and Q. Xu, *J. Phys. Chem. Lett.*, 2014, **5**, 1400-1411.
127. G. Lu, S. Li, Z. Guo, O. K. Farha, B. G. Hauser, X. Qi, Y. Wang, X. Wang, S. Han, X. Liu, J. S. DuChene, H. Zhang, Q. Zhang, X. Chen, J. Ma, S. C. J. Loo, W. D. Wei, Y. Yang, J. T. Hupp and F. Huo, *Nat. Chem.*, 2012, **4**, 310-316.
128. A. Aijaz, A. Karkamkar, Y. J. Choi, N. Tsumori, E. Ronnebro, T. Autrey, H. Shioyama and Q. Xu, *J. Am. Chem. Soc.*, 2012, **134**, 13926-13929.
129. C. Largeot, C. Portet, J. Chmiola, P.-L. Taberna, Y. Gogotsi and P. Simon, *J. Am. Chem. Soc.*, 2008, **130**, 2730-2731.
130. H. Zhang, G. Cao, Y. Yang and Z. Gu, *Carbon*, 2008, **46**, 30-34.
131. D. E. Jiang, Z. H. Jin, D. Henderson and J. Wu, *J. Phys. Chem. Lett.*, 2012, **3**, 1727-1731.
132. L. Zhang, X. Yang, F. Zhang, G. Long, T. Zhang, K. Leng, Y. Zhang, Y. Huang, Y. Ma, M. Zhang and Y. Chen, *J. Am. Chem. Soc.*, 2013, **135**, 5921-5929.
133. Y. Zhang, H. Feng, X. Wu, L. Wang, A. Zhang, T. Xia, H. Dong, X. Li and L. Zhang, *Int. J. Hydrogen Energy*, 2009, **34**, 4889-4899.
134. G. Wang, L. Zhang and J. Zhang, *Chem. Soc. Rev.*, 2012, **41**, 797-828.
135. V. Augustyn, P. Simon and B. Dunn, *Energy Environ. Sci.*, 2014, **7**, 1597-1614.
136. D. Y. Lee, S. J. Yoon, N. K. Shrestha, S.-H. Lee, H. Ahn and S.-H. Han, *Microporous Mesoporous Mater.*, 2012, **153**, 163-165.
137. C. Liao, Y. Zuo, W. Zhang, J. Zhao, B. Tang, A. Tang, Y. Sun and J. Xu, *Russ. J. Electrochem.*, 2012, **49**, 983-986.
138. K. M. Choi, H. M. Jeong, J. Park, Hyo, Y. B. Zhang, J. K. Kang and O. M. Yaghi, *ACS Nano*, 2014, **8**, 7451-7457.
139. A. G. Pandolfo and A. F. Hollenkamp, *J. Power Sources*, 2006, **157**, 11-27.
140. E. Frackowiak and F. Beguin, *Carbon*, 2001, **39**, 937-950.
141. B. Liu, H. Shioyama, H. Jiang, X. Zhang and Q. Xu, *Carbon*, 2010, **48**, 456-463.
142. L. Radhakrishnan, J. Reboul, S. Furukawa, P. Srinivasu, S. Kitagawa and Y. Yamauchi, *Chem. Mater.*, 2011, **23**, 1225-1231.

143. J. W. Jeon, R. Sharma, P. Meduri, B. W. Arey, H. T. Schaef, J. L. Lutkenhaus, J. P. Lemmon, P. K. Thallapally, M. I. Nandasiri, B. P. McGrail and S. K. Nune, *ACS Appl. Mater. Interfaces*, 2014, **6**, 7214-7222.
144. N. L. Torad, R. R. Salunkhe, Y. Li, H. Hamoudi, M. Imura, Y. Sakka, C. C. Hu and Y. Yamauchi, *Chem. Eur. J.*, 2014, **20**, 7895-7900.
145. P. Zhang, F. Sun, Z. Shen and D. Cao, *J. Mater. Chem. A*, 2014, **2**, 12873-12880.
146. X. Yan, X. Li, Z. Yan and S. Komarneni, *Appl. Surf. Sci.*, 2014, **308**, 306-310.
147. F. Zhang, L. Hao, L. J. Zhang and X. G. Zhang, *Int. J. Electrochem. Sci.*, 2011, **6**, 2943 - 2954.
148. Z. Jiang, Z. Li, Z. Qin, H. Sun, X. Jiao and D. Chen, *Nanoscale*, 2013, **5**, 11770-11775.
149. A. D. Roberts, X. Li and H. Zhang, *Chem. Soc. Rev.*, 2014, **43**, 4341-4356.
150. J. Lee, J. Kim and T. Hyeon, *Adv. Mater.*, 2006, **18**, 2073-2094.
151. N. P. Wickramaratne, V. S. Perera, B.-W. Park, M. Gao, G. W. McGimpsey, S. D. Huang and M. Jaroniec, *Chem. Mater.*, 2013, **25**, 2803-2811.
152. B. Dunn, H. Kamath and J.-M. Tarascon, *Science*, 2011, **334**, 928-935.
153. P. G. Bruce, B. Scrosati and J.-M. Tarascon, *Angew. Chem. Int. Ed.*, 2008, **47**, 2930-2946.
154. J. B. Goodenough and Y. Kim, *Chem. Mater.*, 2009, **22**, 587-603.
155. K. Saravanan, M. Nagarathinam, P. Balaya and J. J. Vittal, *J. Mater. Chem.*, 2010, **20**, 8329-8335.
156. L. Hu, N. Yan, Q. Chen, P. Zhang, H. Zhong, X. Zheng, Y. Li and X. Hu, *Chem. Eur. J.*, 2012, **18**, 8971-8977.
157. L. Hu, P. Zhang, H. Zhong, X. Zheng, N. Yan and Q. Chen, *Chem. Eur. J.*, 2012, **18**, 15049-15056.
158. A. Banerjee, V. Aravindan, S. Bhatnagar, D. Mhamane, S. Madhavi and S. Ogale, *Nano Energy*, 2013, **2**, 890-896.
159. A. Banerjee, U. Singh, V. Aravindan, M. Srinivasan and S. Ogale, *Nano Energy*, 2013, **2**, 1158-1163.
160. T. K. Kim, K. J. Lee, J. Y. Cheon, J. H. Lee, S. H. Joo and H. R. Moon, *J. Am. Chem. Soc.*, 2013, **135**, 8940-8946.
161. R. Wu, X. Qian, F. Yu, H. Liu, K. Zhou, J. Wei and Y. Huang, *J. Mater. Chem. A*, 2013, **1**, 11126-11129.
162. Q. Wang, R. Zou, W. Xia, J. Ma, B. Qiu, A. Mahmood, R. Zhao, Y. Yang, D. Xia and Q. Xu, *Small*, 2015, DOI: 10.1002/smll.201403579.
163. J. M. Tarascon and M. Armand, *Nature*, 2001, **414**, 359-367.
164. H. Li and H. Zhou, *Chem. Commun.*, 2012, **48**, 1201-1217.
165. J. Wang and X. Sun, *Energy Environ. Sci.*, 2012, **5**, 5163-5185.
166. J. Jiang, Y. Li, J. Liu and X. Huang, *Nanoscale*, 2011, **3**, 45-58.
167. J. Jiang, Y. Li, J. Liu, X. Huang, C. Yuan and X. W. Lou, *Adv. Mater.*, 2012, **24**, 5166-5180.
168. Z.-S. Wu, G. Zhou, L.-C. Yin, W. Ren, F. Li and H.-M. Cheng, *Nano Energy*, 2012, **1**, 107-131.

169. X. Cao, B. Zheng, X. Rui, W. Shi, Q. Yan and H. Zhang, *Angew. Chem. Int. Ed.*, 2014, **53**, 1404-1409.
170. Y. Han, P. Qi, S. Li, X. Feng, J. Zhou, H. Li, S. Su, X. Li and B. Wang, *Chem. Commun.*, 2014, **50**, 8057-8060.
171. M. Okubo, C. H. Li and D. R. Talham, *Chem. Commun.*, 2014, **50**, 1353-1355.
172. Y. You, X. Wu, Y. Yin and Y. Guo, *Energy Environ. Sci.*, 2014, **7**, 1643-1647.
173. Y. Yue, A. J. Binder, B. Guo, Z. Zhang, Z. A. Qiao, C. Tian and S. Dai, *Angew. Chem. Int. Ed.*, 2014, **53**, 3134-3137.
174. Y. Lu, L. Wang, J. Cheng and J. B. Goodenough, *Chem. Commun.*, 2012, **48**, 6544-6546.
175. C. D. Wessells, R. A. Huggins and Y. Cui, *Nat. Commun.*, 2011, **2**, 550.
176. L. Wang, Y. Lu, J. Liu, M. Xu, J. Cheng, D. Zhang and J. B. Goodenough, *Angew. Chem. Int. Ed.*, 2013, **52**, 1964-1967.
177. P. G. Bruce, S. A. Freunberger, L. J. Hardwick and J.-M. Tarascon, *Nat. Mater.*, 2012, **11**, 19-29.
178. J. R. Akridge, Y. V. Mikhaylik and N. White, *Solid State Ionics*, 2004, **175**, 243-245.
179. X. Ji, K. T. Lee and L. F. Nazar, *Nat. Mater.*, 2009, **8**, 500-506.
180. J. Schuster, G. He, B. Mandlmeier, T. Yim, K. T. Lee, T. Bein and L. F. Nazar, *Angew. Chem. Int. Ed.*, 2012, **51**, 3591-3595.
181. S. Xin, L. Gu, N. H. Zhao, Y. X. Yin, L. J. Zhou, Y. G. Guo and L. J. Wan, *J. Am. Chem. Soc.*, 2012, **134**, 18510-18513.
182. J. T. Lee, Y. Zhao, S. Thieme, H. Kim, M. Oschatz, L. Borchardt, A. Magasinski, W. I. Cho, S. Kaskel and G. Yushin, *Adv. Mater.*, 2013, **25**, 4573-4579.
183. C. Zhang, H. B. Wu, C. Yuan, Z. Guo and X. W. D. Lou, *Angew. Chem. Int. Ed.*, 2012, **51**, 9592-9595.
184. R. Demir-Cakan, M. Morcrette, F. Nouar, C. Davoisne, T. Devic, D. Gonbeau, R. Dominko, C. Serre, G. Férey and J.-M. Tarascon, *J. Am. Chem. Soc.*, 2011, **133**, 16154-16160.
185. G. Ferey, C. Serre, C. Mellot-Draznieks, F. Millange, S. Surble, J. Dutour and I. Margiolaki, *Angew. Chem. Int. Ed.*, 2004, **43**, 6296-6301.
186. Z. Wang, X. Li, Y. Cui, Y. Yang, H. Pan, Z. Wang, C. Wu, B. Chen and G. Qian, *Cryst. Growth Des.*, 2013, **13**, 5116-5120.
187. Z. Wang, Z. Dou, Y. Cui, Y. Yang, Z. Wang and G. Qian, *Microporous Mesoporous Mater.*, 2014, **185**, 92-96.
188. J. Zheng, J. Tian, D. Wu, M. Gu, W. Xu, C. Wang, F. Gao, M. H. Engelhard, J. Zhang, J. Liu and J. Xiao, *Nano Lett.*, 2014, **14**, 2345-2352.
189. J. Zhou, R. Li, X. Fan, Y. Chen, R. Han, W. Li, J. Zheng, B. Wang and X. Li, *Energy Environ. Sci.*, 2014, **7**, 2715-2724.
190. Z. Zhao, S. Wang, R. Liang, Z. Li, Z. Shi and G. Chen, *J. Mater. Chem. A*, 2014, **2**, 13509-13512.
191. Y. Yue, B. Guo, Z.-A. Qiao, P. F. Fulvio, J. Chen, A. J. Binder, C. Tian and S. Dai, *Microporous Mesoporous Mater.*, 2014, **198**, 139-143.
192. H. B. Wu, S. Wei, L. Zhang, R. Xu, H. H. Hng and X. W. Lou, *Chem. Eur. J.*, 2013, **19**, 10804-10808.

193. X. Wang, X. Fang, X. Guo, Z. Wang and L. Chen, *Electrochim. Acta*, 2013, **97**, 238-243.
194. K. Xi, S. Cao, X. Peng, C. Ducati, R. V. Kumar and A. K. Cheetham, *Chem. Commun.*, 2013, **49**, 2192-2194.
195. G. Xu, B. Ding, L. Shen, P. Nie, J. Han and X. Zhang, *J. Mater. Chem. A*, 2013, **1**, 4490-4496.
196. M. Winter and R. J. Brodd, *Chem. Rev.*, 2004, **104**, 4245-4269.
197. B. C. H. Steele and A. Heinzel, *Nature*, 2001, **414**, 345-352.
198. M. K. Debe, *Nature*, 2012, **486**, 43-51.
199. S. Guo, S. Zhang and S. Sun, *Angew. Chem. Int. Ed.*, 2013, **52**, 8526-8544.
200. I. E. L. Stephens, A. S. Bondarenko, U. Gronbjerg, J. Rossmeisl and I. Chorkendorff, *Energy Environ. Sci.*, 2012, **5**, 6744-6762.
201. C. Sealy, *Mater. Today*, 2008, **11**, 65-68.
202. G. Wu, K. L. More, C. M. Johnston and P. Zelenay, *Science*, 2011, **332**, 443-447.
203. R. Jasinski, *Nature*, 1964, **201**, 1212-1213.
204. J. P. Dodelet, *in N4-Macrocyclic Metal Complexes, ed. J. H.Zagal, F. Bedioui and J. P. Dodelet, Springer, New York, 2006, pp. 83-147.*, 2006.
205. M. Lefevre, E. Proietti, F. Jaouen and J. P. Dodelet, *Science*, 2009, **324**, 71-74.
206. R. Bashyam and P. Zelenay, *Nature*, 2006, **443**, 63-66.
207. F. Jaouen, M. Lefevre, J. P. Dodelet and M. Cai, *J. Phys. Chem. B*, 2006, **110**, 5553-5558.
208. J. Mao, L. Yang, P. Yu, X. Wei and L. Mao, *Electrochem. Commun.*, 2012, **19**, 29-31.
209. M. Jahan, Z. Liu and K. P. Loh, *Adv. Funct. Mater.*, 2013, **23**, 5363-5372.
210. M. Jiang, L. Li, D. Zhu, H. Zhang and X. Zhao, *J. Mater. Chem. A*, 2014, **2**, 5323-5329.
211. M. Jahan, Q. Bao and K. P. Loh, *J. Am. Chem. Soc.*, 2012, **134**, 6707-6713.
212. H. Tang, H. Yin, J. Wang, N. Yang, D. Wang and Z. Tang, *Angew. Chem. Int. Ed.*, 2013, **52**, 5585-5589.
213. S. Ma, G. A. Goenaga, A. V. Call and D. J. Liu, *Chem. Eur. J.*, 2011, **17**, 2063-2067.
214. F. Jaouen, J. Herranz, M. Lefevre, J. P. Dodelet, U. I. Kramm, I. Herrmann, P. Bogdanoff, J. Maruyama, T. Nagaoka, A. Garsuch, J. R. Dahn, T. Olson, S. Pylypenko, P. Atanassov and E. A. Ustinov, *ACS Appl. Mater. Interfaces*, 2009, **1**, 1623-1639.
215. D. Zhao, J. L. Shui, C. Chen, X. Chen, B. M. Reprogle, D. Wang and D. J. Liu, *Chem. Sci.*, 2012, **3**, 3200-3205.
216. L. Zhang, Z. Su, F. Jiang, L. Yang, J. Qian, Y. Zhou, W. Li and M. Hong, *Nanoscale*, 2014, **6**, 6590-6602.
217. E. Proietti, F. Jaouen, M. Lefevre, N. Larouche, J. Tian, J. Herranz and J. P. Dodelet, *Nat. Commun.*, 2011, **2**, 416.
218. J. Tian, A. Morozan, M. T. Sougrati, M. Lefevre, R. Chenitz, J. P. Dodelet, D. Jones and F. Jaouen, *Angew. Chem. Int. Ed.*, 2013, **52**, 6867-6870.
219. W. Xia, J. Zhu, W. Guo, L. An, D. Xia and R. Zou, *J. Mater. Chem. A*, 2014, **2**, 11606-11613.

220. H. X. Zhong, J. Wang, Y. W. Zhang, W. L. Xu, W. Xing, D. Xu, Y. F. Zhang and X. B. Zhang, *Angew. Chem. Int. Ed.*, 2014, **53**, 14235-14239.
221. W. Zhang, Z. Y. Wu, H. L. Jiang and S. H. Yu, *J. Am. Chem. Soc.*, 2014, **136**, 14385-14388.
222. M. G. Walter, E. L. Warren, J. R. McKone, S. W. Boettcher, Q. Mi, E. A. Santori and N. S. Lewis, *Chem. Rev.*, 2010, **110**, 6446-6473.
223. J. H. Yang, D. E. Wang, H. X. Han and C. Li, *Acc. Chem. Res.*, 2013, **46**, 1900-1909.
224. D. Merki and X. Hu, *Energy Environ. Sci.*, 2011, **4**, 3878-3888.
225. K. F. Babu, M. A. Kulandainathan, I. Katsounaros, L. Rassaei, A. D. Burrows, P. R. Raithby and F. Marken, *Electrochem. Commun.*, 2010, **12**, 632-635.
226. B. Nohra, H. El Moll, L. M. Rodriguez Albelo, P. Mialane, J. Marrot, C. Mellot-Draznieks, M. O'Keeffe, R. Ngo Biboum, J. Lemaire, B. Keita, L. Nadjo and A. Dolbecq, *J. Am. Chem. Soc.*, 2011, **133**, 13363-13374.
227. Y. Gong, T. Wu, P. G. Jiang, J. H. Lin and Y. X. Yang, *Inorg. Chem.*, 2013, **52**, 777-784.
228. Y. Gong, Z. Hao, J. Meng, H. Shi, P. Jiang, M. Zhang and J. Lin, *ChemPlusChem*, 2014, **79**, 266-277.
229. H. Wang, F. Yin, G. Li, B. Chen and Z. Wang, *Int. J. Hydrogen Energy*, 2014, **39**, 16179-16186.
230. T. Y. Ma, S. Dai, M. Jaroniec and S. Z. Qiao, *J. Am. Chem. Soc.*, 2014, **136**, 13925-13931.
231. N. Agmon, *Chem. Phys. Lett.*, 1995, **244**, 456-462.
232. K.-D. Kreuer, *Chem. Mater.*, 1996, **8**, 610-641.
233. Z. Ma and M. E. Tuckerman, *Chem. Phys. Lett.*, 2011, **511**, 177-182.
234. M. E. Tuckerman, D. Marx and M. Parrinello, *Nature*, 2002, **417**, 925-929.
235. S. Kanda, K. Yamashita and K. Ohkawa, *Bull. Chem. Soc. Jpn.*, 1979, **52**, 3296-3301.
236. H. Kitagawa, Y. Nagao, M. Fujishima, R. Ikeda and S. Kanda, *Inorg. Chem. Commun.*, 2003, **6**, 346-348.
237. Y. Nagao, R. Ikeda, K. Iijima, T. Kubo, K. Nakasuji and H. Kitagawa, *Synth. Met.*, 2003, **135-136**, 283-284.
238. H. Okawa, A. Shigematsu, M. Sadakiyo, T. Miyagawa, K. Yoneda, M. Ohba and H. Kitagawa, *J. Am. Chem. Soc.*, 2009, **131**, 13516-13522.
239. T. Yamada, M. Sadakiyo and H. Kitagawa, *J. Am. Chem. Soc.*, 2009, **131**, 3144-3145.
240. E. Pardo, C. Train, G. Gontard, K. Boubekeur, O. Fabelo, H. Liu, B. Dkhil, F. Lloret, K. Nakagawa, H. Tokoro, S. Ohkoshi and M. Verdaguer, *J. Am. Chem. Soc.*, 2011, **133**, 15328-15331.
241. A. Shigematsu, T. Yamada and H. Kitagawa, *J. Am. Chem. Soc.*, 2011, **133**, 2034-2036.
242. B. M. Wiers, M.-L. Foo, N. P. Balsara and J. R. Long, *J. Am. Chem. Soc.*, 2011, **133**, 14522-14525.
243. N. C. Jeong, B. Samanta, C. Y. Lee, O. K. Farha and J. T. Hupp, *J. Am. Chem. Soc.*, 2012, **134**, 51-54.
244. M. Sadakiyo, H. Kasai, K. Kato, M. Takata and M. Yamauchi, *J. Am. Chem. Soc.*, 2014, **136**, 1702-1705.

245. Y. Nagao, M. Fujishima, R. Ikeda, S. Kanda and H. Kitagawa, *Synth. Met.*, 2003, **133-134**, 431-432.
246. M. Sadakiyo, T. Yamada and H. Kitagawa, *J. Am. Chem. Soc.*, 2009, **131**, 9906-9907.
247. S.-i. Ohkoshi, K. Nakagawa, K. Tomono, K. Imoto, Y. Tsunobuchi and H. Tokoro, *J. Am. Chem. Soc.*, 2010, **132**, 6620-6621.
248. H. Ōkawa, M. Sadakiyo, T. Yamada, M. Maesato, M. Ohba and H. Kitagawa, *J. Am. Chem. Soc.*, 2013, **135**, 2256-2262.
249. S. Bureekaew, S. Horike, M. Higuchi, M. Mizuno, T. Kawamura, D. Tanaka, N. Yanai and S. Kitagawa, *Nat. Mater.*, 2009, **8**, 831-836.
250. J. A. Hurd, R. Vaidhyanathan, V. Thangadurai, C. I. Ratcliffe, I. L. Moudrakovski and G. K. H. Shimizu, *Nat. Chem.*, 2009, **1**, 705-710.
251. S. Li, Z. Zhou, Y. Zhang, M. Liu and W. Li, *Chem. Mater.*, 2005, **17**, 5884-5886.
252. S. S. Nagarkar, S. M. Unni, A. Sharma, S. Kurungot and S. K. Ghosh, *Angew. Chem. Int. Ed.*, 2014, **53**, 2638-2642.

Table of contents

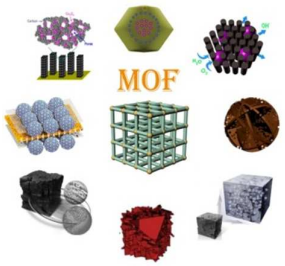

This review presents a summary of recent progress and strategies in fabricating MOF-based nanostructures for electrochemical applications.

Broader Context

Metal-organic frameworks (MOFs) represent one of the best examples of materials fabricated from molecular engineering with high surface areas, tunable porosity, inherent presence of coordinated metal and heteroatoms. Fabricating MOF-based nanostructures for electrochemical applications is a newly developed but fast growing field, which has shown huge impact on development of state-of-the-art Li-ion batteries, supercapacitors and fuel cells. The flexibility of designing and fabricating MOFs enable MOF-derived materials with tunable composition and texture, based on the needs of modern electrochemical devices. In this review, we summarize the recent progresses from application-based designing of MOFs to the synthesis of various nanostructures using MOFs as template/sacrificial materials.